

# CO<sub>2</sub> and HCl emissions from Popocatépetl volcano: Supplementary Material

Wolfgang Stremme<sup>1,\*</sup>, Michel Grutter<sup>1,\*</sup>, Jorge Baylón<sup>1</sup>, Noemie Taquet<sup>1</sup>, Alejandro Bezanilla<sup>1</sup>, Eddy Plaza-Medina<sup>1</sup>, Benedetto Schiavo<sup>1</sup>, Claudia Rivera<sup>1</sup>, Thomas Blumenstock<sup>2</sup> and Frank Hase<sup>2</sup>

<sup>1</sup>Instituto de Ciencias de la Atmosfera y Cambio Climatico, Universidad Nacional Autonoma de Mexico

<sup>2</sup>Institute for Meteorology and Climate Research, Karlsruhe Institute of Technology, Germany

The supplementary material contains a sequence of photos of the 26 de April 2015 and additional information about technical details, regarding the analysis of the spectra, reconstruction of flux and ratios and quality control of the events, as well as a set of tables and graphics of all events which has been analysed for the flux calculation or composition analysis:

- Section 1 contains photos about the volcanic plume on 26 of April, on which a extraordinary strong HCl-emission but a very normal CO<sub>2</sub>/HCl ratio was found.
- Section 2 shows difference between the CO<sub>2</sub> retrieval results of the spectra in this work and using the default spectra calculated by the OPUS-software. Only a small difference or improvement is visible due to a correction of the variation in the solar intensity during the measurement.
- How the sensitivity of the retrieval strategy has been optimized to quantify CO<sub>2</sub> anomalies in the altitude of the Popocatépetl volcano is described in Sec.3.
- Technically detail airmass dependence (solar zenith angle dependence) is given in Sec.4.
- Section 5 contains the set of ratios which documents the quality control which excluded only one CO<sub>2</sub>/HCl ratio out of 25 analysed events.
- Section 6 presents a correlation plot and the estimation of the overall ratio between SO<sub>2</sub> and HCl using the HCl-retrieval of this work.
- The last section (Sec. 7) reports all HCl-flux measurements and how quality control was realized to select a subset of days with short HCl time series for the calculation of the average HCl-flux.

## 1 SEQUENCE OF PHOTOS OF THE PLUME EVENT ON 26 OF APRIL 2015



**Figure S1.** Sequence of photos taken at 6:24, 6:42, 6:52 and 7:00 on 26 April 2015 at the Altzomoni observatory.

The sequence of photos in Figure S1 shows a passive degassing plume of Popocatépetl in the early morning. On this day (25 April 2022) the highest vertical HCl column and volcanic gas anomaly has been

detected in the four years. We see a constant degassing plume containing small puff with apparently higher density of volcanic gas. Therefore a high variability in flux and composition is very likely. The side view to the volcano crater and plume shows that the plume equilibrates a little bit above the crater short after a initial ascending phase.

## 2 FOURIER TRANSFORMATION USING CALPY

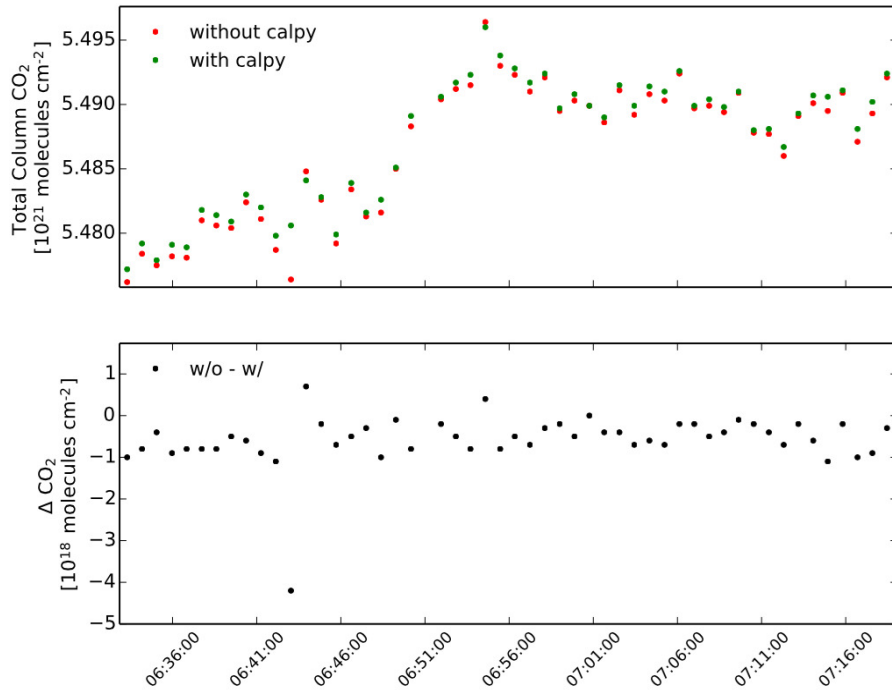


**Figure S2.** CO<sub>2</sub> vertical columns retrieved with a scaling retrieval from spectra in Altzomoni: Upper panel: Retrieval from spectra calculated by OPUS software without DC-correction (red) and retrieved from spectra Fourier transformed and DC corrected using the CALPY software (green). Lower panel shows the differences between both retrievals: At the moment when the volcanic plume enters the line of sight a small difference can be observed in the variance of consecutive measurements. The retrieval from the corrected spectra show less scatter than the uncorrected spectra. This effect might be expected, however the difference of 4E18 molec./cm<sup>2</sup> / 5.5E21 molec./cm<sup>2</sup> is less than 0.08% and comparable small.

In Fourier Transform Spectroscopy interferograms are recorded as raw data. In Altzomoni we commonly use the spectra generated imidiately after adquisition and the Fourier-transformation is calculated by the OPUS software from Bruker. The solar intensity variation due to thin clouds is visible in the DC-interferogram and in our site only used for an initial quality controll. (Keppel-Aleks et al., 2007) showed that the observing of solar intensity fluctuation can be corrected and used to improve the quality of the spectra. The interferograms recorded in this work contains a forward and a backward scan, so that no scans are averaged and the DC-correction might be corrected efficiently. The corresponding routines of the software package CALPY (Kiel et al., 2016) is used to correct the interferograms and to Fourier transform the corrected interferograms to spectra again offline. A very small difference in the retrieved CO<sub>2</sub> columns (scaling retrieval) from the CALPY-spectra used in this work and the OPUS-specta Baylon et al. (2017) can be observed for the small time series around the volcanic plume event on 26 of April 2015. The average difference of -3.8E18 molec./cm<sup>2</sup> is 0.07 % of the vertical column of CO<sub>2</sub> in Altzomoni. The scatter of the difference (CALPY-OPUS) is roughly estimated around 5E17 molec./cm<sup>2</sup> and therefore

around 0.01% of the total vertical column and ten times smaller as the precision (0.1%) of the CO<sub>2</sub> and the typical measurement noise error. This very small improvement helps however among other strategies to improve the analysis and reduce errorbars. DC-correction according to (Keppel-Aleks et al., 2007) is state of the art in the TCCON and COCCON-network and therefore applied. However up to now other errors as the signal noise error are still dominant, and we do not discuss the improvement due to the DC-correction in the main article. The systematic difference of -3.8E18 mole./cm<sup>2</sup> is less than 0.08% and probably due to numerical issues or slightly differences in the phase correction of the interferogram.

### 3 VERTICAL SENSITIVITY AND QUANTIFICATION

To quantify correctly the enhancement of a trace gas the retrieved column should have a sensitivity of one in the altitude in which the gas anomaly is located. There are different retrieval strategies to realize this purpose for volcanic gases with the retrieval code PROFFIT (Taquet et al., 2019). For the purpose to quantify the anomaly of CO<sub>2</sub>, which is located in the altitude of 6 km, a layer of the concentrations of 4-8 km is shifted to fit the spectrum, similar as Butz et al. (2017), normal scaling of the whole profile leads to a overestimation by up to 40%, if the solar zenith angle is rather large as on the 26 April 2015, on which the detection on the volcanic event occurred very early in the morning. If the fitted layer is only 4-6 km, (center of mass slightly below 5 km) the sensibility in the altitude of 6 km, depends slightly on the solar zenith angle. Therefore the shift of the CO<sub>2</sub> concentrations in a larger or smaller layer tunes the vertical sensitivity distribution (Averaging Kernel for total columns). For the finally chosen strategy, the different sensitivities show a common crossing point (a knot) at a sensitivity of 1.0, near the altitude where most frequently the volcanic plume is expected. This has two advantages: i) The retrieved CO<sub>2</sub> ratio can be used without correction factor as the sensitivity is almost 1.0 and ii) the fact that there is a common crossing point of the vertical sensitivity functions means that the ratio of different events recorded by different solar zenith angles can be compared directly.

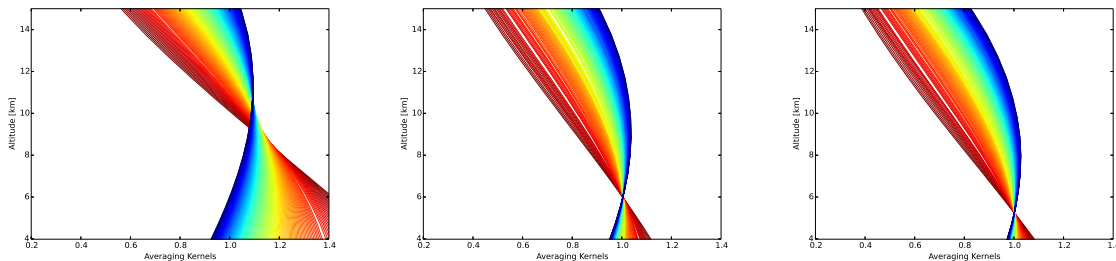


**Figure S3.** Dependence of sensitivity on solar zenith angle for three different regularisations. left: scaling of the whole profile; center: scaling of the levels below 8 km; right: scaling of the level below 6 km. The constraint results in a sensitivity in the altitude in which the volcanic plume is expected of around 1 for all solar zenith angles, as desired for a harmonized analysis of plume events of different solar zenith angles.

### 4 AIRMASS DEPENDENCE OF CO<sub>2</sub>

The CO<sub>2</sub> column retrieval shows an airmass dependence, which is already well known and is empirical corrected in the TCCON network (Wunch et al., 2011). For this study we do not need exactitude or network precision for the total vertical CO<sub>2</sub> column, as we are not interested of compare the CO<sub>2</sub> measurement with insitu-measurements, model studies, neither with other sites nor with our own data of another volcanic event, we just want a constant background CO<sub>2</sub> column, which allows us to derive the CO<sub>2</sub> anomaly

produced by a single volcanic event. Finally we are doing so, by fitting a polynomial, a typical strategy which works as a high-pass filter, to eliminate the solar zenith dependence. As described by the manuscript as strategy (iii) a small part of the random error could be eliminated as it correlates with the retrieved O<sub>2</sub> anomaly. The resulting CO<sub>2</sub> anomaly is small in that the dominating error is the noise while systematic errors from spectroscopy are here irrelevant. Fitting a solar zenith dependence as done by (Butz et al., 2017) is straight forward, nevertheless, we give in this section of the supplemental part a kind of explanation why there is the airmass dependence and how we could avoid it.

$$\vec{x}_{ret} - \vec{x}_{apr} = AK_{sza}(x_{true} - \vec{x}_{apr}) + \vec{\epsilon} \quad (\text{S1})$$

$$col_{ret} = a_{sza}^T(x_{true} - \vec{x}_{apr}) + \underbrace{col_{apr} + \sigma_{col}}_{\text{const and independent of sza}} \quad (\text{S2})$$

The column total  $a_{sza}^T = g^T \cdot AK_{sza}$  is calculated from the the total column operator  $g^T$  and the averaging kernel for profiles  $AK_{sza}$ , if  $AK_{sza}$  and the profile  $\vec{x}$  are described in the units of partial columns, the total column operator has the simple form  $g^T = (111\dots)$ . As the averaging kernel for total columns depends systematically on the solar zenith angle, we actually expect in general a solar zenith angle dependence if  $\vec{x}_{true} - \vec{x}_{apr}$  is constant but not zero. Only if we have chosen  $\vec{x}_{apr} = \vec{x}_{true}$  the equation should be independent from  $a_{sza}^T$ . The general consensus is that the actual CO<sub>2</sub> spectroscopy used in this work are not sufficient precise so that a forward simulation with the true atmospheric state does not produce the correct spectrum. However there might be an atmospheric state which simulates the correct spectrum better  $\vec{x}_{apr-best}$ , at least for an interval of solar zenith angles.

As we are more interested in the true anomaly than the true atmospheric state, we just aim to get a state  $\vec{x}_{apr-best}$ , which finally would simulate the spectra for the given background spectra and help us to calculate the anomaly.

$$\vec{x}_{ret} - \vec{x}_{apr-best} = \text{Gain} \left[ \vec{y}_{measured} - \vec{F}(\vec{x}_{ret}) + R(\vec{x}_{ret} - \vec{x}_{apr-best}) \right] \quad (\text{S3})$$

$$\text{Gain} \left[ \vec{y}_{measured} - \vec{F}(\vec{x}_{apr-best}) + R(\vec{x}_{apr-best} - \vec{x}_{apr-best}) \right] = \text{Gain} [\vec{\epsilon}] \quad (\text{S4})$$

The way how to find the vector  $\vec{x}_{apr-best}$  is an ill posed problem, and as we are interested in column anomalies we start from Equation S1, but for columns:

$$col_{apr-best} - col_{apr} = a_{sza}^T(\vec{x}_{apr-best} - \vec{x}_{apr}) + \sigma_{col} \quad (\text{S5})$$

for a set of different sza angles we could write a set of equations:

$$\underbrace{\begin{pmatrix} \Delta col_{apr}(sza = 70^\circ) \\ \vdots \\ \Delta col_{apr}(sza = 85^\circ) \end{pmatrix}}_{:= \vec{y}} = \underbrace{\begin{pmatrix} a_{70^\circ}^1 & \cdots & a_{70^\circ}^{44} \\ \vdots & \ddots & \vdots \\ a_{85^\circ}^1 & \cdots & a_{85^\circ}^{44} \end{pmatrix}}_{\mathbf{K} :=} \cdot \underbrace{\begin{pmatrix} \Delta x_{apr}^1 \\ \vdots \\ \Delta x_{apr}^{44} \end{pmatrix}}_{\delta \vec{x} =} \quad (\text{S6})$$

We find the solution  $\vec{x}$  ( $\delta x_{apr}$ ), by constrained least square fitting using a Tikhonov L1 constraint  $R = \lambda L_1^T L_1$  to get a rather smoothed corrected a priori profile.

$$\Delta \vec{x}_{apr} = (\mathbf{K}^T \mathbf{K} + \mathbf{R})^{-1} \mathbf{K}^T \Delta \vec{col}_{apr} \quad (\text{S7})$$

For the column we get just the measurement error and as the  $a^T$  is around one in the height of the volcanic plume, as we optimized for this purpose the retrieval strategy by adjusting the concentrations of a 4-8km layer. For the true state and the retrieved state we write following relation:

$$\vec{x}_{plume}^{true} = \vec{x}^{true} - \vec{x}_{background} \quad (\text{S8})$$

$$\vec{x}_{plume}^{ret} = \vec{x}^{ret} - \vec{x}_{apr} \quad (\text{S9})$$

$$\delta col_{volcano} := g^T \vec{x}_{plume} \quad (\text{S10})$$

$$a^T \vec{x}_{plume} \approx g^T \vec{x}_{plume}^{true} = \delta col_{volcano}^{true} \quad (\text{S11})$$

$$col_{ret} - col_{apr-best} = \delta col_{volcano} + \sigma \quad (\text{S12})$$

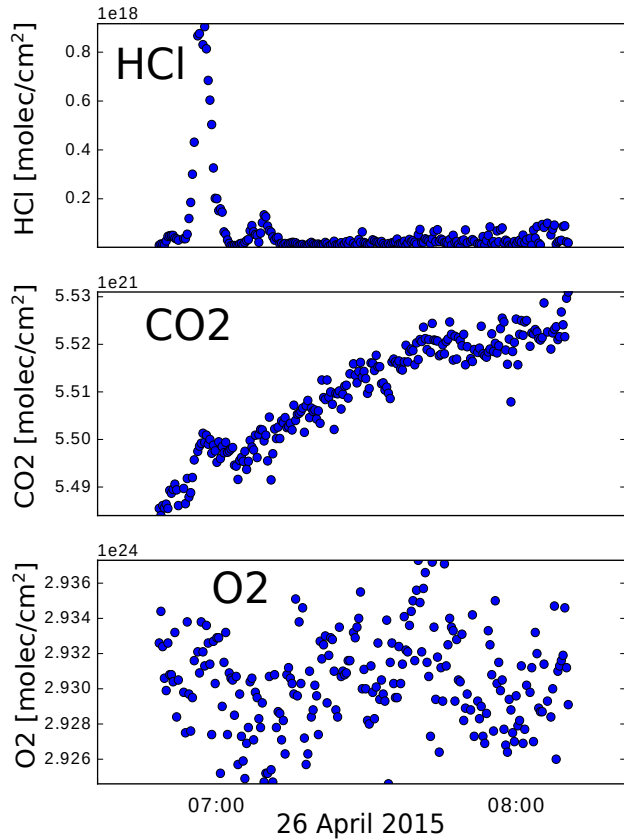


**Figure S4.** Time series of the retrieved vertical columns from spectra recorded at the 26 of April 2015 in Altzomoni. Vertical HCl column (upper panel), Vertical CO<sub>2</sub> column (panel in the middle) and O<sub>2</sub> column lower panel. The CO<sub>2</sub>-retrieval uses the a priori of 400 ppm which results in a solar dependence.

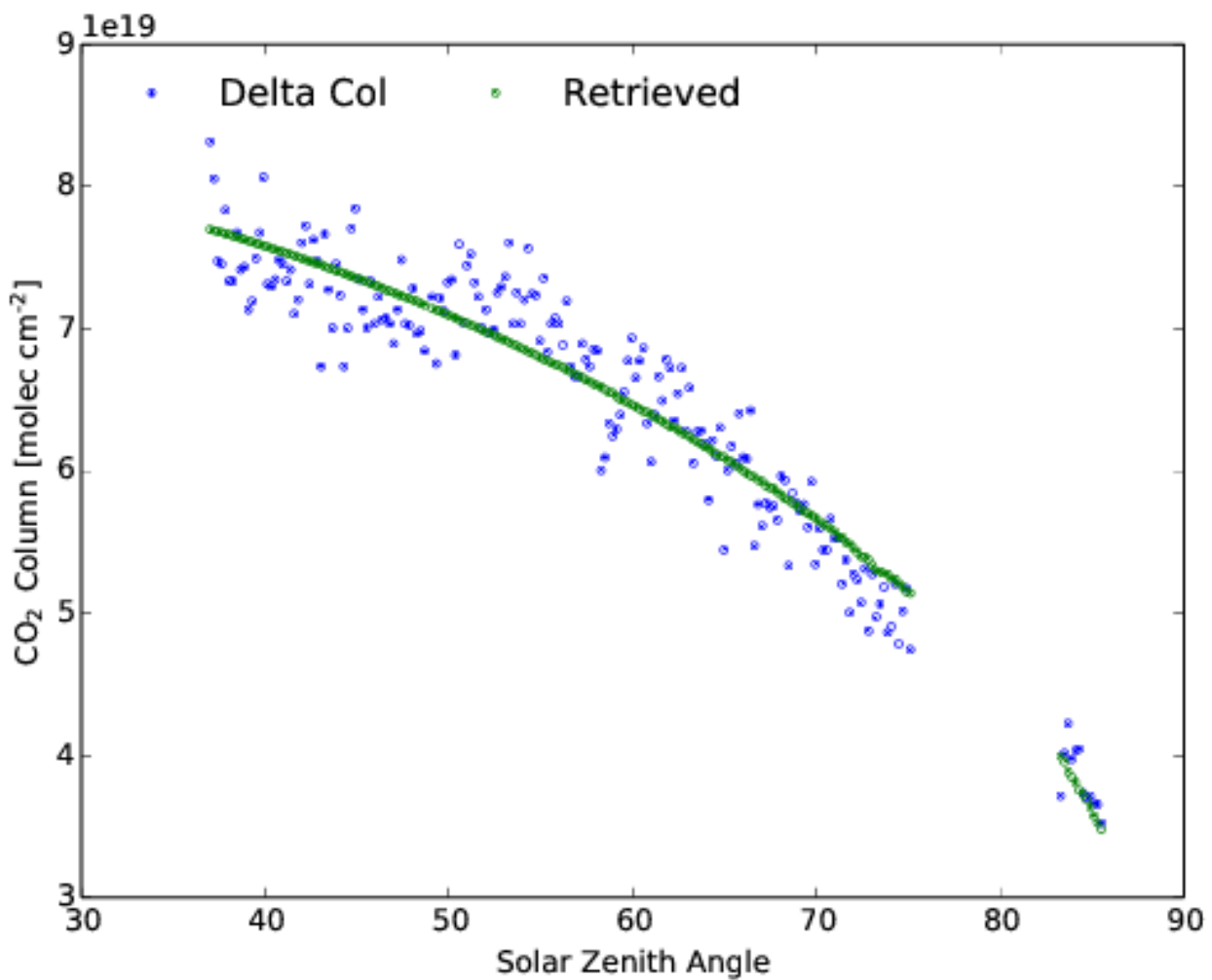


**Figure S5.** Airmass dependence on 26 of April 2015: As the vertical column sensitivity depends on solar zenith angle (astronomical airmass), we can tune the airmass dependence by the choose of an a priori profile.

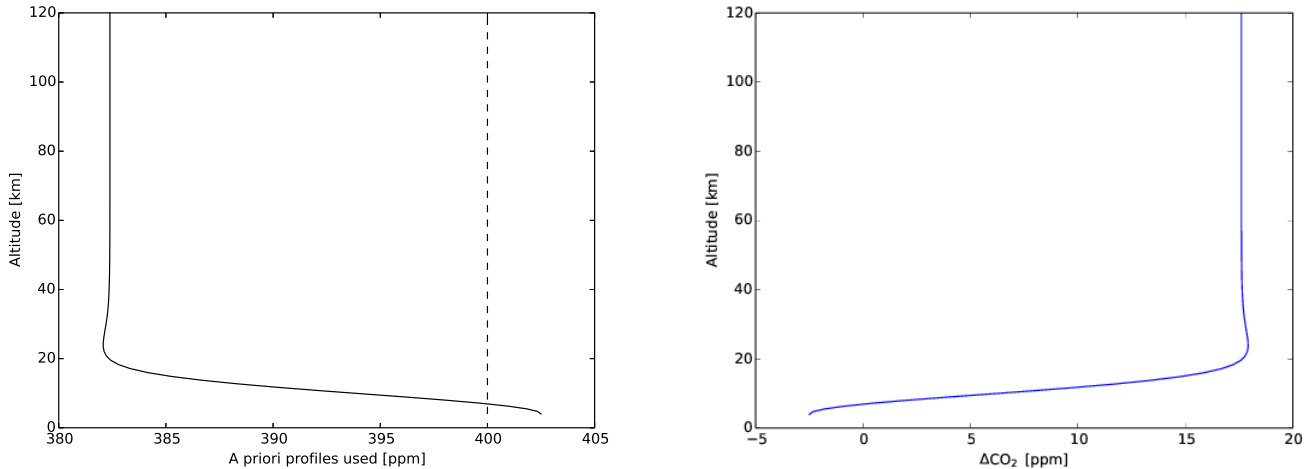


**Figure S6.** Airmass dependence on 26 of April 2015: As the vertical column sensitivity depends on solar zenith angle (astronomical airmass), we can tune the airmass dependence by the choose of an a priori profile.

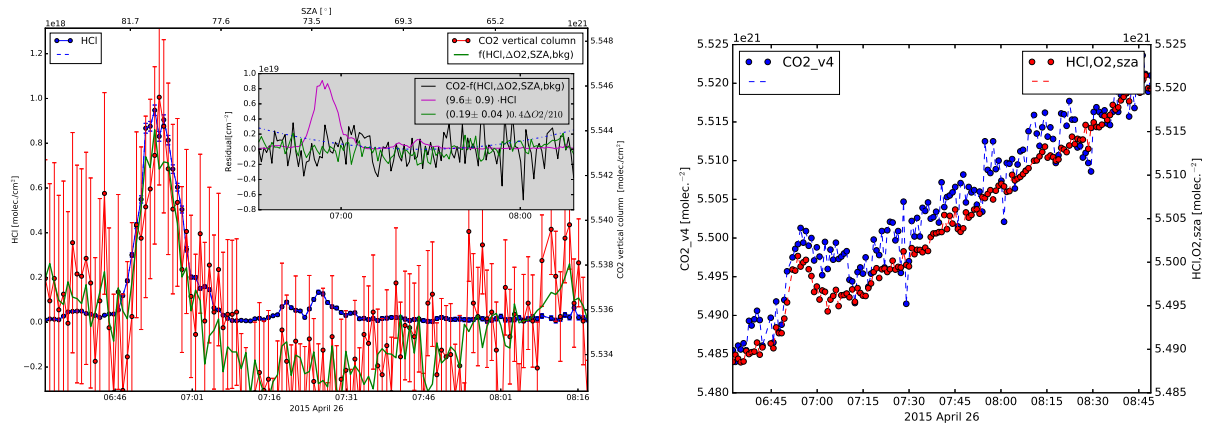


**Figure S7.** left panel,  $\text{CO}_2$  retrieval with "optimized" a priori show no linear dependence on the solar zenith angle (airmass dependence),  $\text{O}_2$  and resulting air mass dependence are of the magnitude of the HCl plume at the center of the time window (around 7:20) but 10 times smaller than the volcanic HCl signal at around 6:50. Right panel: same time serie of retrieved (red) and fitted (blue)  $\text{CO}_2$  columns. The  $\text{CO}_2$  retrievals uses a simple standard apriori (400 ppm in each altitude), so that the linear SZA and airmass dependence is dominant. The fitted time series (blue) has its own y-axis, which is slightly shifted below, so that the points of both time series can be observed. The curve is a linear combination of the retrieved HCl column, the retrieved  $\text{O}_2$  anomaly a constant background and a linear and squared solar zenith angle dependence. This strategy is applied to all 25 events where a HCl/ $\text{CO}_2$  ratio might be retrieved.

## 5 CO<sub>2</sub>/HCl RATIOS AND QUALITY CONTROL

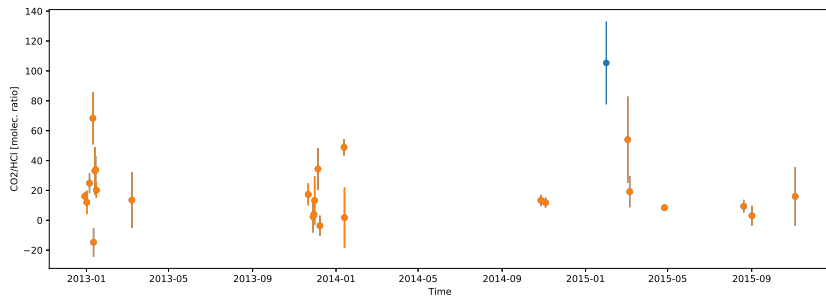


**Figure S8.** Time series of the HCl/CO<sub>2</sub> ratios. The blue marked event has been excluded for the calculation of the average.

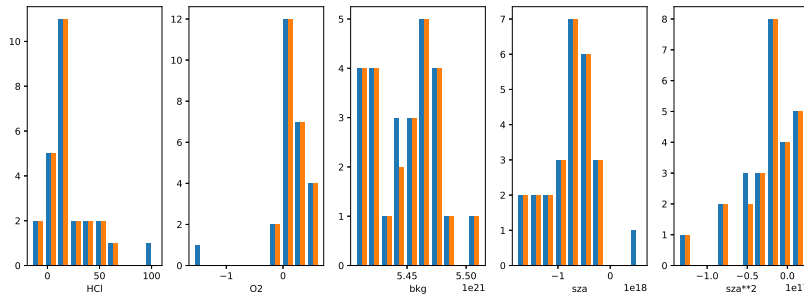


**Figure S9.** Histogram of fitparameters: CO<sub>2</sub>/HCl ratio, correlative error with O<sub>2</sub>, background, linear and square solar zenith dependence.

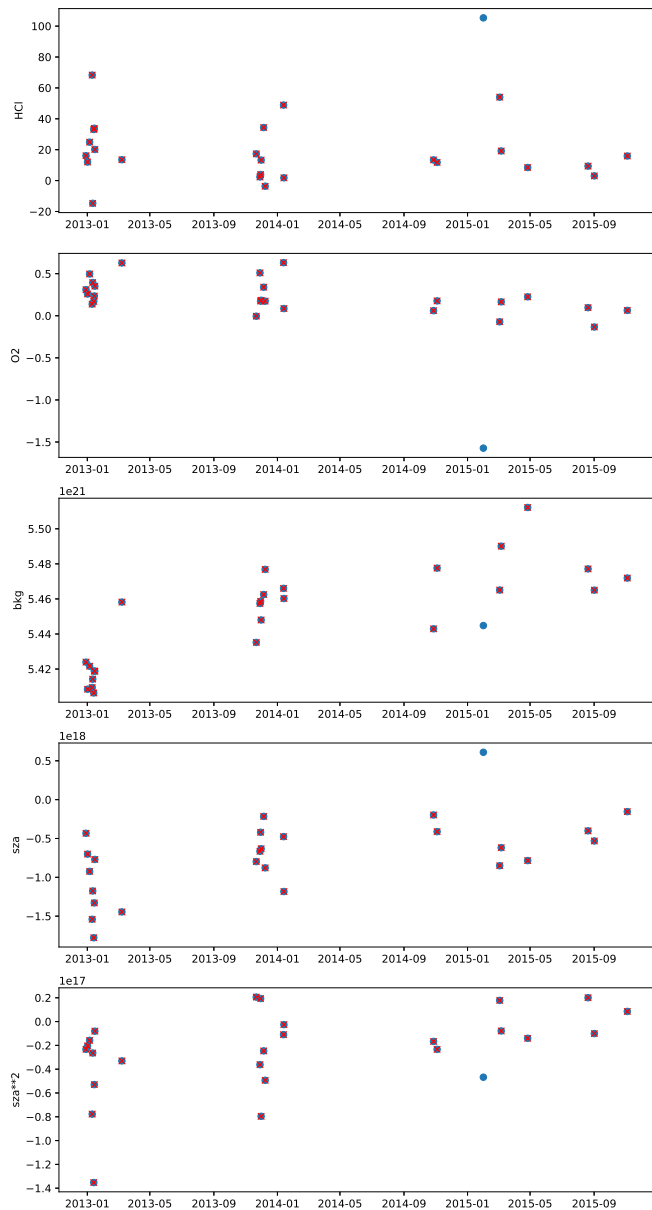


**Figure S10.** Time series of all 5 fit parameter (from top to bottom):  $\text{CO}_2/\text{HCl}$  ratio (HCl), parameter  $\alpha$  ( $\text{O}_2$ ), constant  $\text{co}_2$  background, linear zenith angle dependence quadratic sza-dependence.

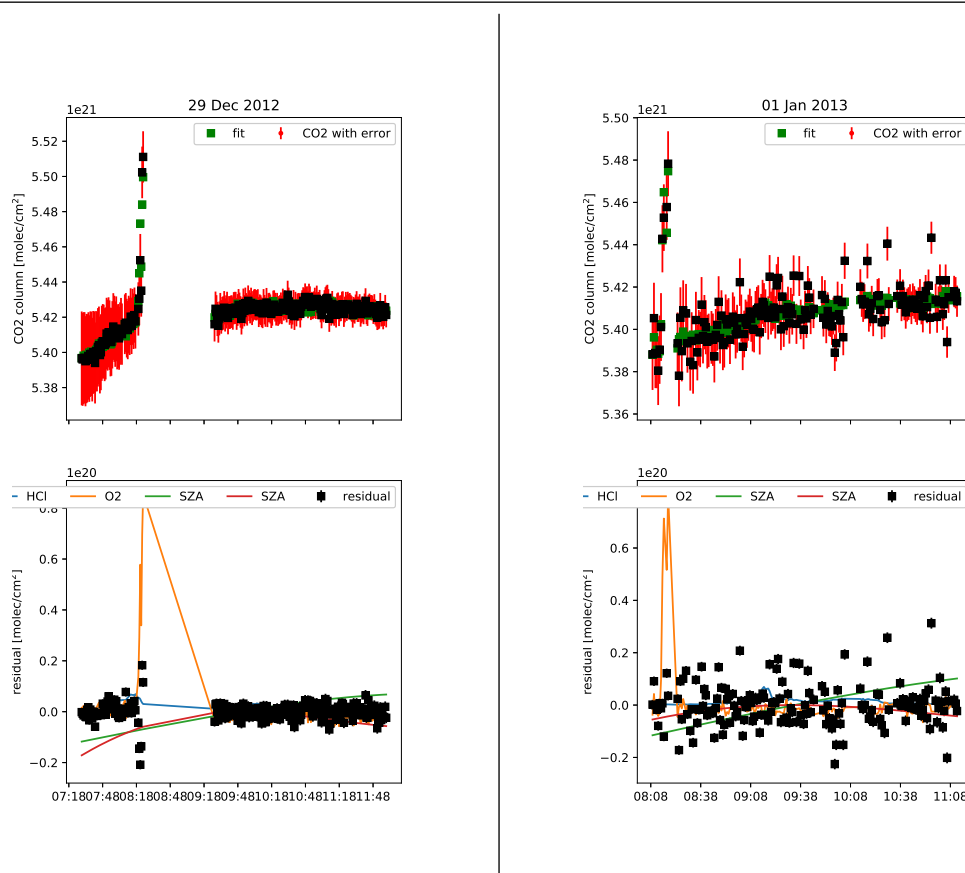


**Figure S11.** Time series of  $\text{CO}_2$  vertical column and reconstruction of  $\text{CO}_2/\text{HCl}$  ratio. Left: 20121229; Right: 20130101; upper panel: measured and simulated time series, lower panel: residual and contributions.

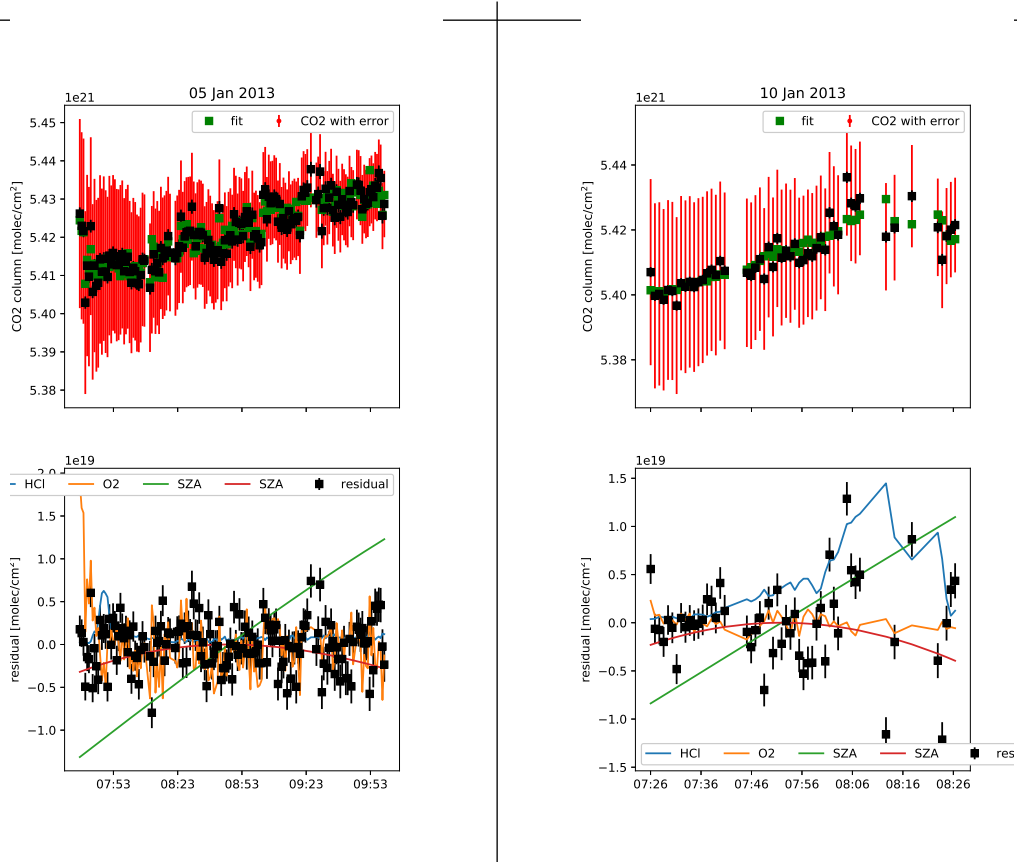


**Figure S12.** Time series of CO<sub>2</sub> vertical column and reconstruction of CO<sub>2</sub>/HCl ratio.

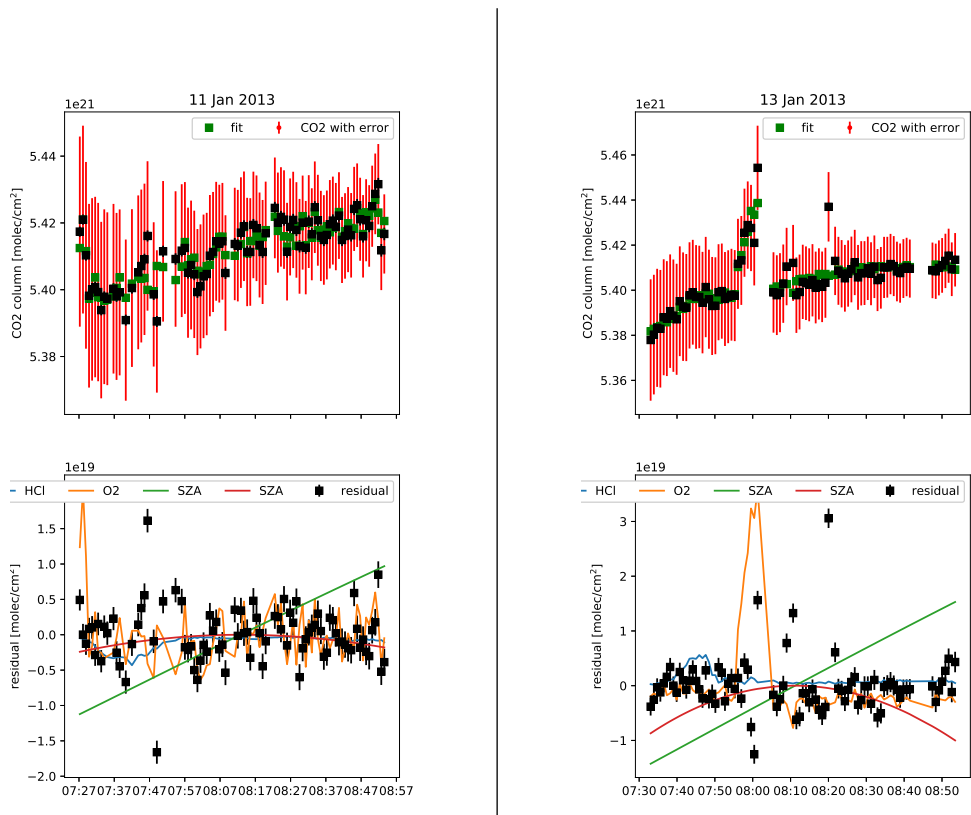


**Figure S13.** Same as Fig.S11, but for (left) and right). left: right:

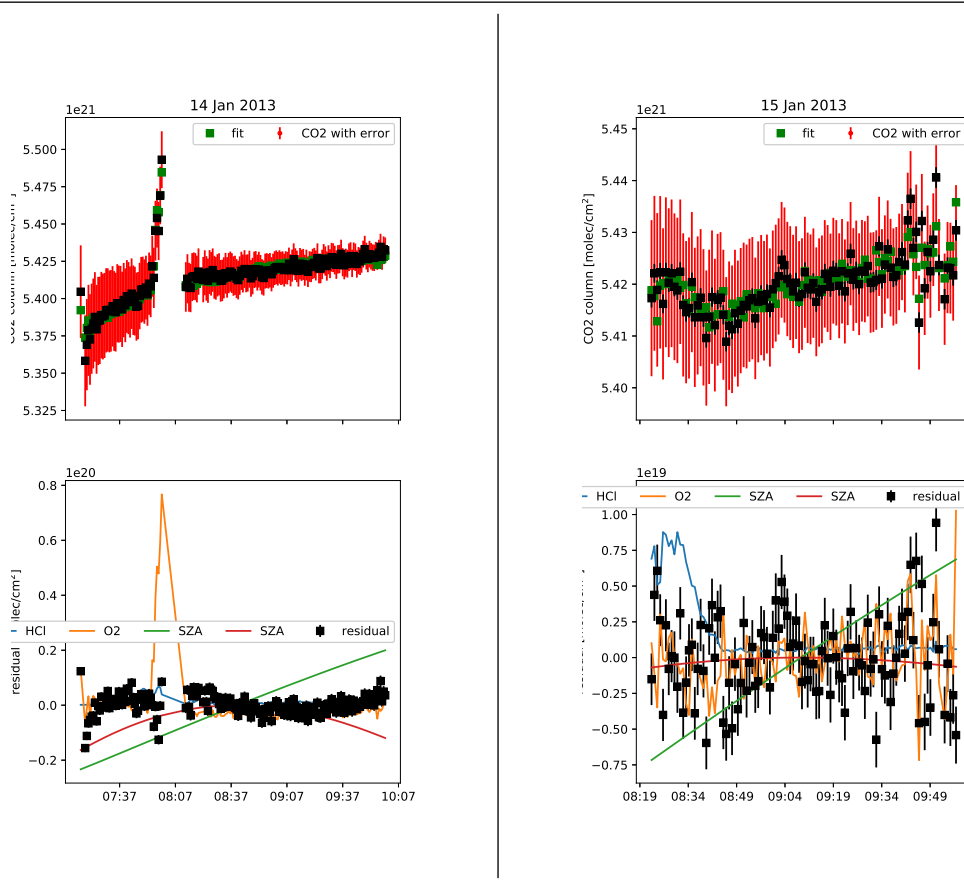


**Figure S14.** Same as Fig.S11, but for (left) and right).

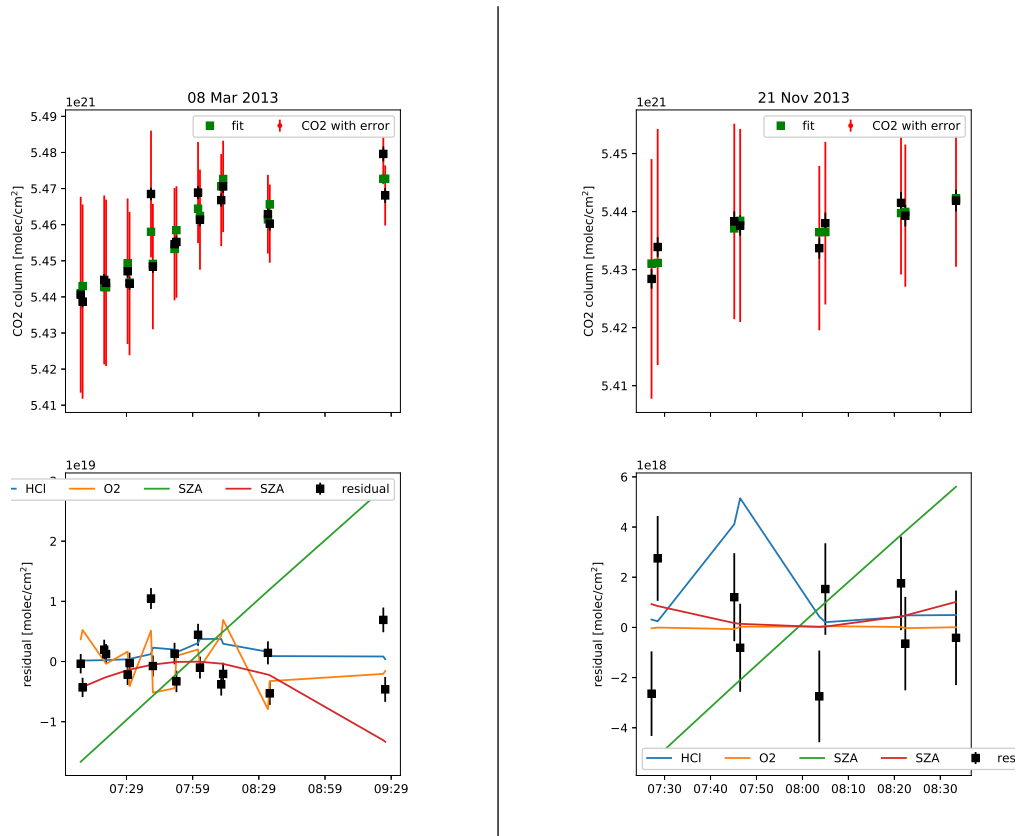


**Figure S15.** Same as Fig.S11, but for (left) and right). left: right:

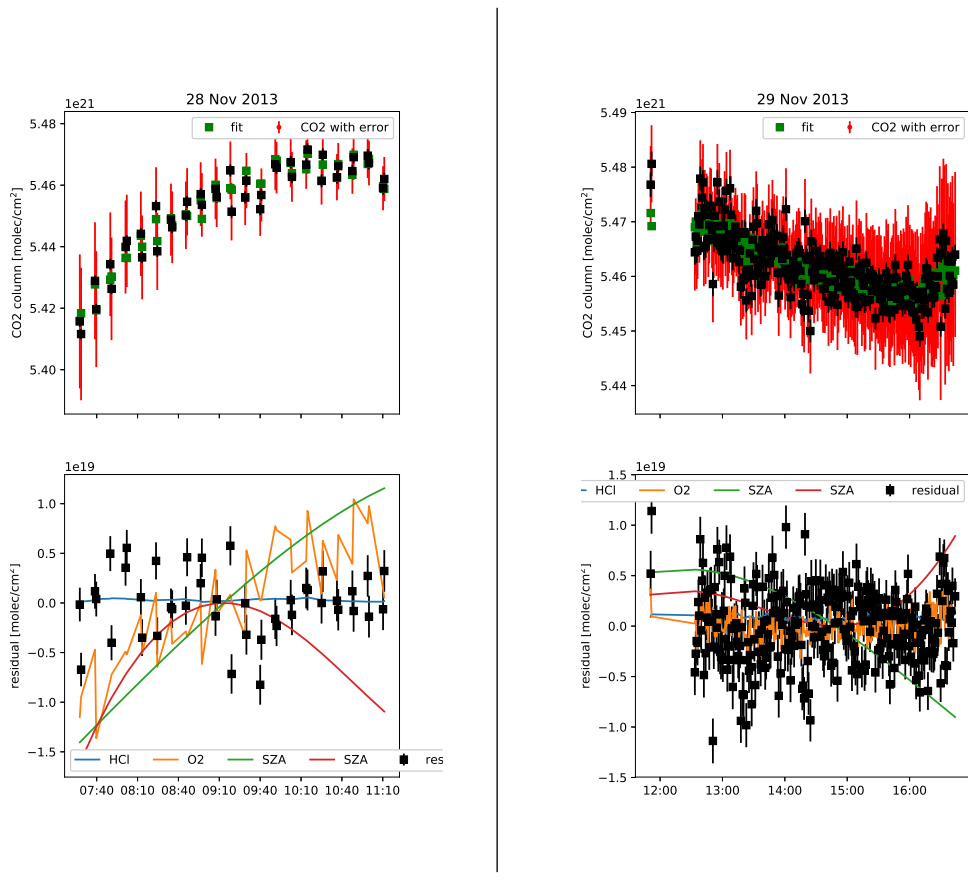


**Figure S16.** Same as Fig.S11, but for (left) and right).

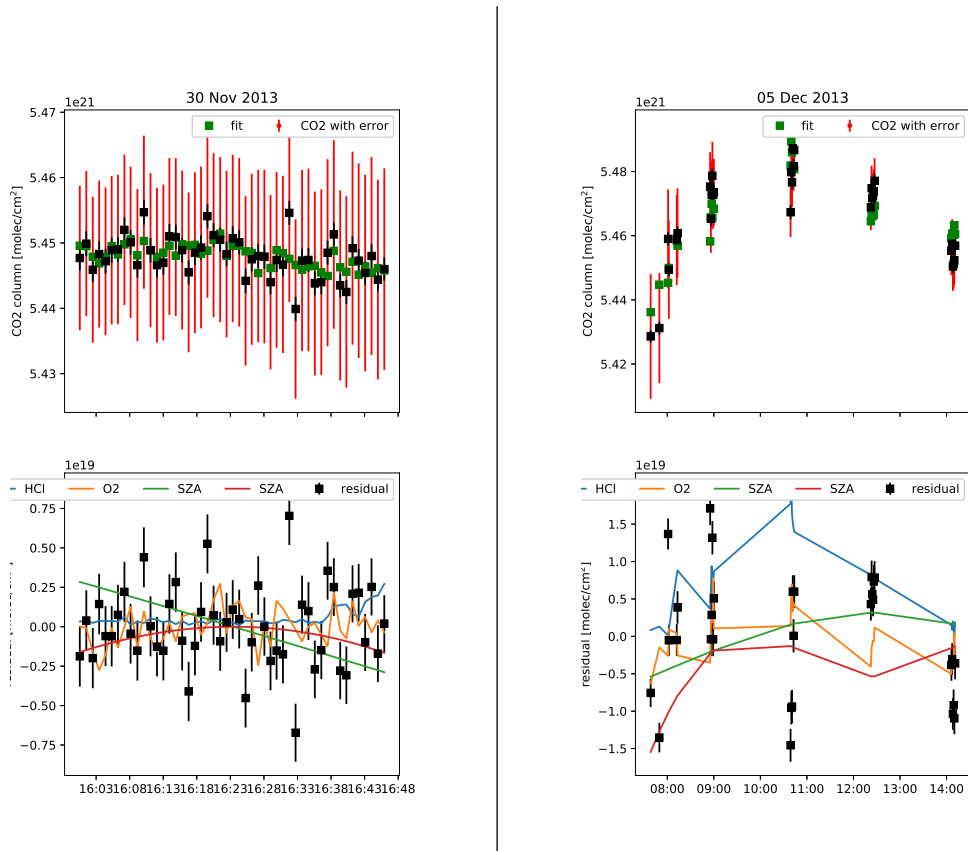


**Figure S17.** Same as Fig.S11, but for (left) and right). left: right:

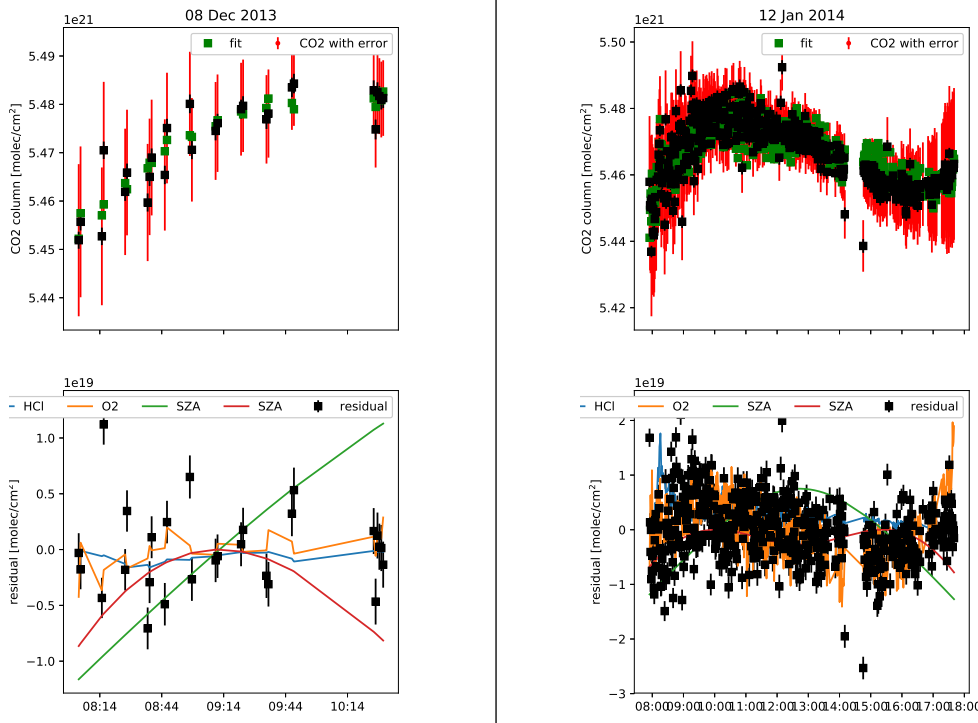


**Figure S18.** Same as Fig.S11, but for (left) and right).

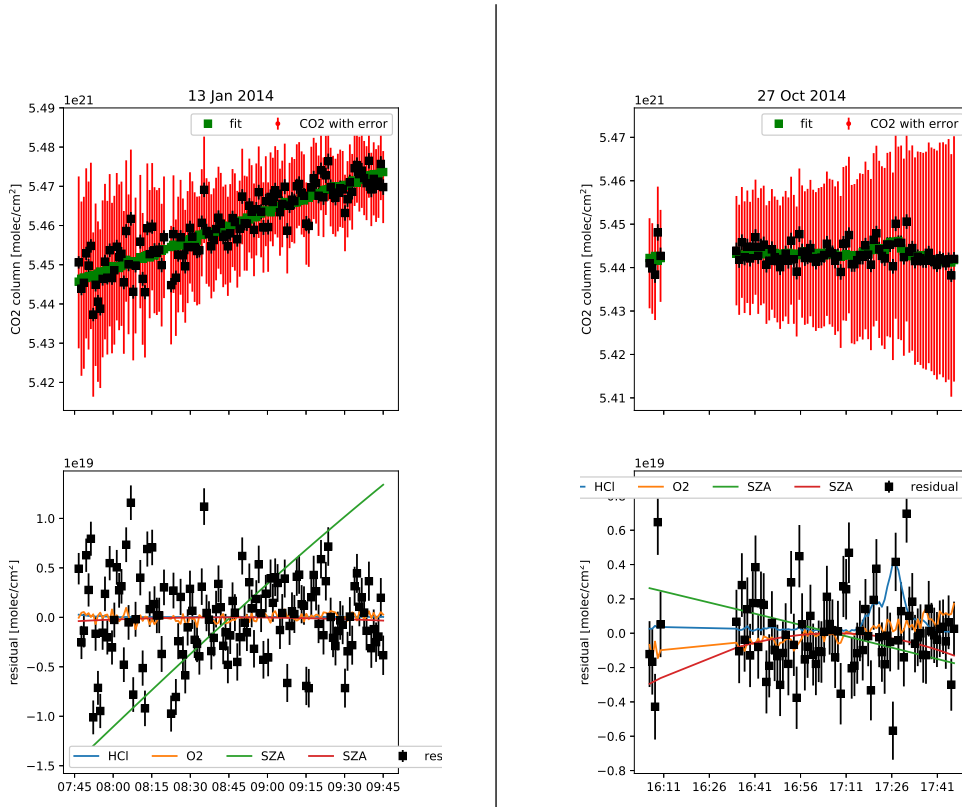


**Figure S19.** Same as Fig.S11, but for (left) and right). left: right:

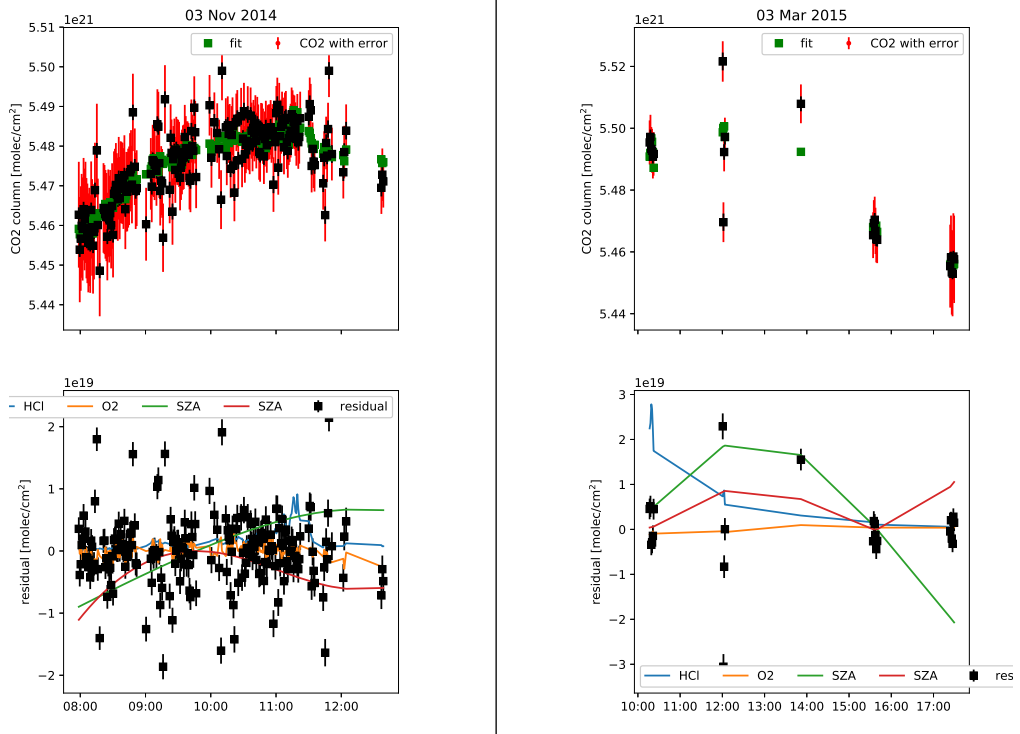


**Figure S20.** Same as Fig.S11, but for (left) and right).

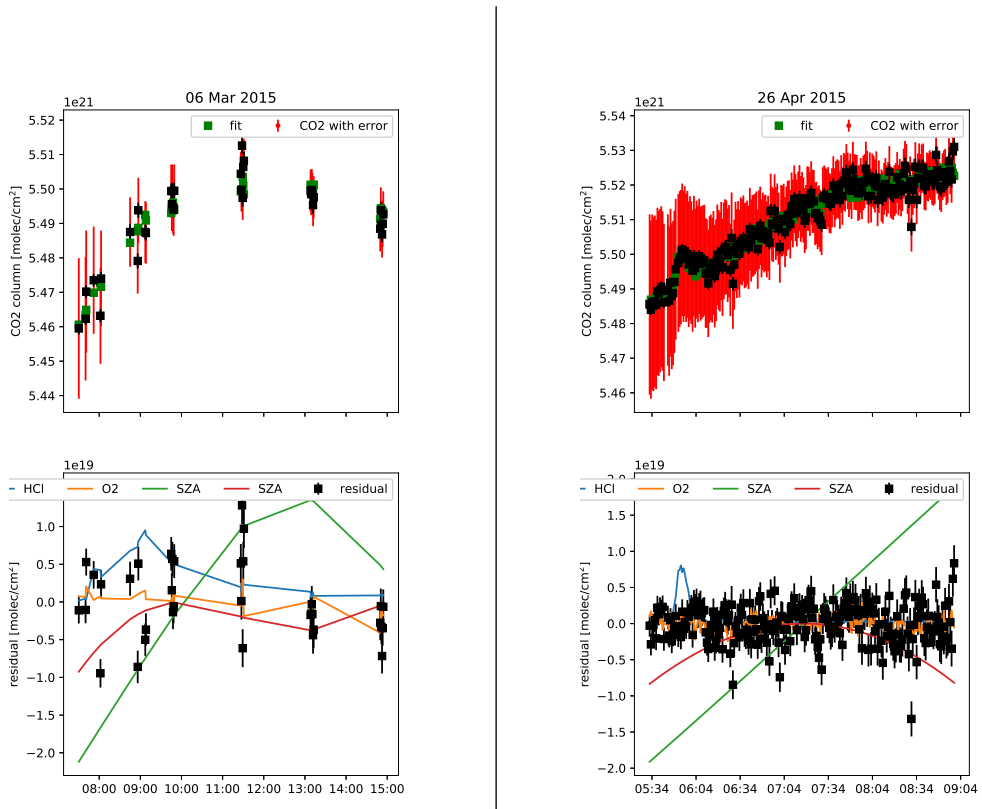


**Figure S21.** Same as Fig.S11, but for (left) and right). left: right:

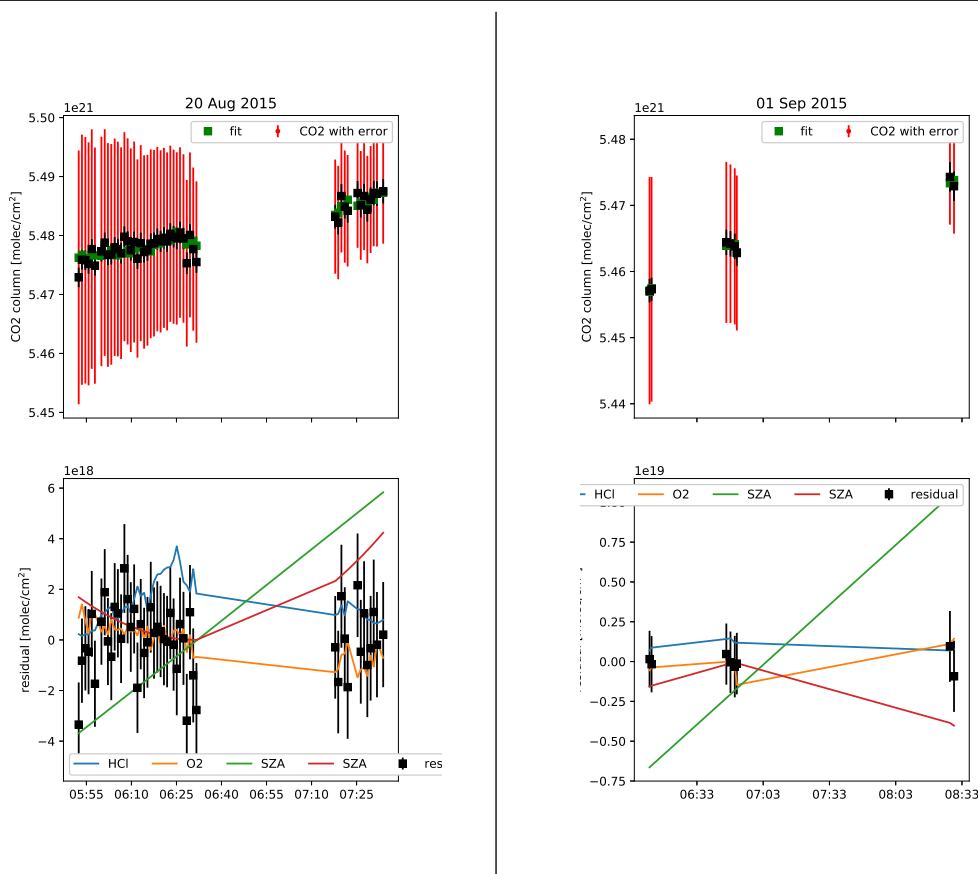


**Figure S22.** Same as Fig.S11, but for (left) and right).

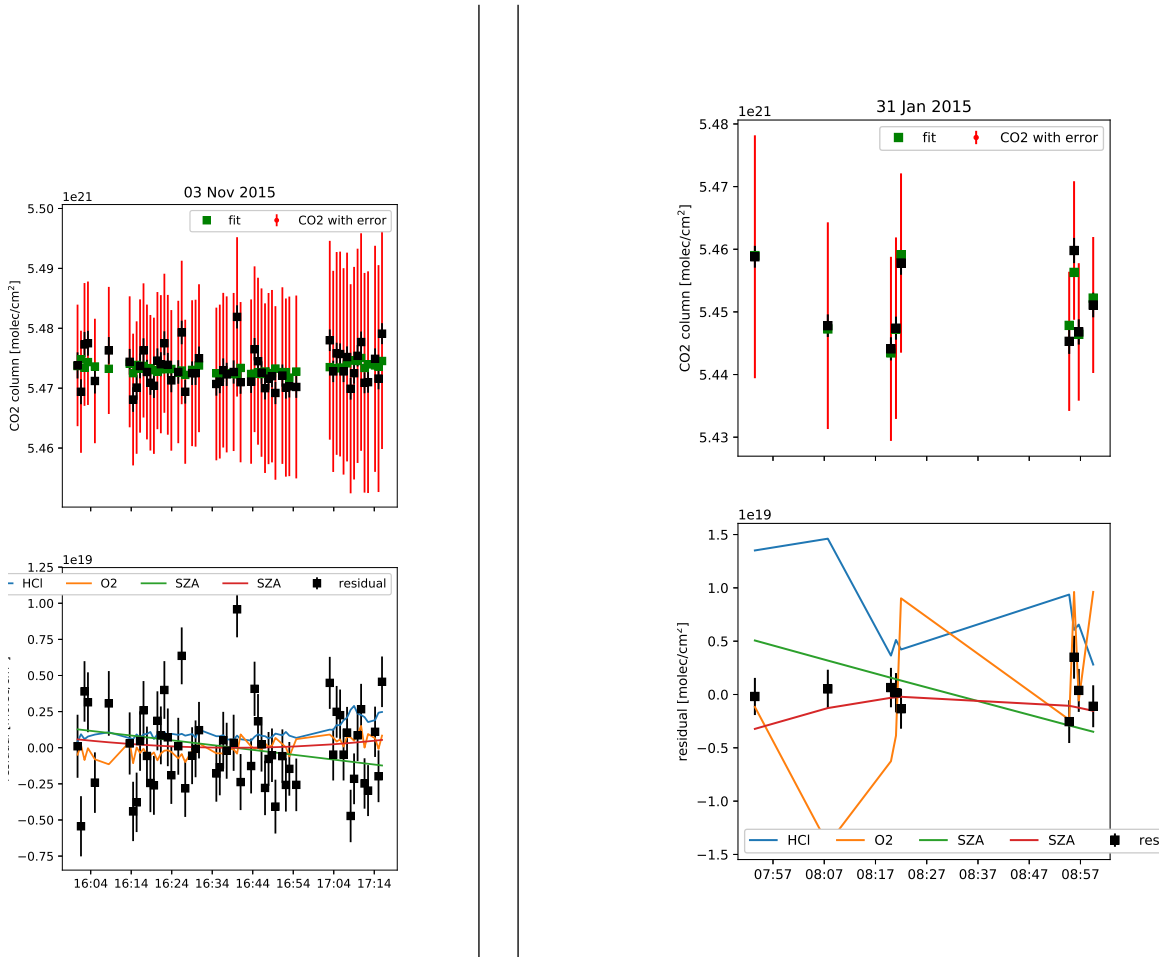


**Figure S23.** Same as Fig.S11, but for (left and (right)). The event on the right hand side is excluded for the analysis.: The fit of the curve results in a negative  $\alpha$ , which represents a negative correlation error between  $\text{O}_2$  and  $\text{CO}_2$ , this artefact indicates that there is something wrong. The few measurements and its distribution with around 5 groups of points are not enough to fit the linear function of 5 parameters. We exclude this event for the calculation of a mean value.

date	time	$\frac{\Delta CO_2}{HCl}$	$\frac{\Delta CO_2}{\Delta O_2}$	const	SZA [molec./cm <sup>-2</sup> ] $\frac{[molec./cm^{-2}]}{degree}$	SZA [molec./cm <sup>-2</sup> ] $\frac{[molec./cm^{-2}]}{degree^2}$
		molec. ratio	$\times \frac{400ppm}{21\%}$	[molec./cm <sup>-2</sup> ]		
20121229	07:29-11:59	16.10 ± 2.98	0.31 ± 0.01	5.42e+21 ± 6.03e+17	-4.33e+17 ± 2.59e+16	-2.33e+16 ± 1.67e+15
20130101	08:09-11:11	12.02 ± 7.88	0.26 ± 0.02	5.41e+21 ± 1.72e+18	-7.01e+17 ± 7.00e+16	-2.04e+16 ± 1.13e+16
20130105	07:37-09:59	24.87 ± 6.72	0.50 ± 0.03	5.42e+21 ± 3.64e+17	-9.24e+17 ± 2.99e+16	-1.58e+16 ± 4.47e+15
20130110	07:26-08:26	68.31 ± 17.52	0.14 ± 0.11	5.41e+21 ± 1.46e+18	-1.54e+18 ± 2.64e+17	-7.78e+16 ± 4.96e+16
20130111	07:27-08:53	-14.71 ± 9.61	0.39 ± 0.05	5.41e+21 ± 7.56e+17	-1.18e+18 ± 9.99e+16	-2.64e+16 ± 2.07e+16
20130113	07:33-08:53	33.08 ± 15.97	0.17 ± 0.01	5.41e+21 ± 9.73e+17	-1.78e+18 ± 1.31e+17	-1.35e+17 ± 2.75e+16
20130114	07:16-09:59	33.87 ± 9.19	0.24 ± 0.01	5.42e+21 ± 5.67e+17	-1.33e+18 ± 3.04e+16	-5.30e+16 ± 3.50e+15
20130115	08:22-09:57	20.14 ± 5.10	0.35 ± 0.05	5.42e+21 ± 4.29e+17	-7.70e+17 ± 9.11e+16	-8.06e+15 ± 1.80e+16
20130308	07:08-09:26	13.52 ± 18.75	0.63 ± 0.17	5.46e+21 ± 3.43e+18	-1.45e+18 ± 2.18e+17	-3.30e+16 ± 1.76e+16
20131121	07:27-08:33	17.33 ± 7.35	-0.01 ± 0.10	5.44e+21 ± 1.46e+18	-7.98e+17 ± 1.41e+17	2.06e+16 ± 4.27e+16
20131128	07:27-11:11	2.36 ± 10.58	0.51 ± 0.09	5.46e+21 ± 1.64e+18	-6.65e+17 ± 8.25e+16	-3.62e+16 ± 4.38e+15
20131129	11:50-16:43	3.95 ± 3.58	0.17 ± 0.03	5.46e+21 ± 8.76e+17	-4.20e+17 ± 2.33e+16	1.94e+16 ± 2.40e+15
20131130	16:00-16:45	13.27 ± 16.11	0.18 ± 0.06	5.45e+21 ± 5.95e+17	-6.32e+17 ± 1.99e+17	-7.96e+16 ± 8.36e+16
20131205	07:38-14:11	34.34 ± 14.11	0.34 ± 0.22	5.46e+21 ± 3.83e+18	-2.16e+17 ± 1.57e+17	-2.46e+16 ± 1.36e+16
20131208	08:03-10:31	-3.63 ± 6.75	0.17 ± 0.11	5.48e+21 ± 1.95e+18	-8.78e+17 ± 1.27e+17	-4.93e+16 ± 1.31e+16
20140112	07:54-17:40	48.89 ± 5.50	0.63 ± 0.03	5.47e+21 ± 5.04e+17	-4.76e+17 ± 2.17e+16	-1.10e+16 ± 1.73e+15
20140113	07:46-09:45	1.80 ± 20.10	0.09 ± 0.09	5.46e+21 ± 6.60e+17	-1.18e+18 ± 5.74e+16	-2.57e+15 ± 1.09e+16
20141027	16:06-17:46	13.39 ± 3.73	0.06 ± 0.05	5.44e+21 ± 3.67e+17	-1.97e+17 ± 1.02e+17	-1.67e+16 ± 6.97e+15
20141103	07:58-12:38	11.79 ± 3.49	0.18 ± 0.06	5.48e+21 ± 7.78e+17	-4.12e+17 ± 4.53e+16	-2.33e+16 ± 3.89e+15
<b>20150131</b>	<b>07:53-08:59</b>	<b>1.05e+02±2.78e+01</b>	<b>-1.57 ± 0.18</b>	<b>5.44e+21±1.42e+18</b>	<b>6.10e+17±1.33e+17</b>	<b>-4.68e+16±4.52e+16</b>
20150303	10:16-17:29	54.00 ± 28.84	-0.07 ± 0.41	5.47e+21 ± 6.73e+18	-8.51e+17 ± 1.33e+17	1.78e+16 ± 1.07e+16
20150306	07:30-14:54	19.17 ± 10.43	0.17 ± 0.14	5.49e+21 ± 3.16e+18	-6.18e+17 ± 7.40e+16	-7.88e+15 ± 4.68e+15
20150426	06:32-09:59	8.46 ± 1.25	0.23 ± 0.04	5.51e+21 ± 2.62e+17	-7.85e+17 ± 1.32e+16	-1.40e+16 ± 1.05e+15
20150820	06:52-08:33	9.38 ± 4.34	0.10 ± 0.05	5.48e+21 ± 1.33e+18	-4.01e+17 ± 8.93e+16	2.01e+16 ± 1.06e+16
20150901	07:11-09:29	3.06 ± 6.63	-0.13 ± 0.07	5.47e+21 ± 3.19e+18	-5.32e+17 ± 3.76e+16	-1.01e+16 ± 6.78e+15
20151103	16:00-17:15	15.93 ± 19.62	0.06 ± 0.06	5.47e+21 ± 1.13e+18	-1.54e+17 ± 1.56e+17	8.53e+15 ± 2.51e+16
<b>20121229-20151103</b>				18.427 ± 12.27	simple average	
molecule ratio		<b>11.422 ± 4.42</b>		average weighted by the errors		
weight ratio		<b>13.787 ± 5.34</b>		average weighted by the errors		

**Table S1.** All events for which HCl/CO<sub>2</sub> ratio was reconstructed. The rather large error dominates the variability and produces even negative values for the ratio. We calculate the weighted average including also negative ratios and weight the individual measurements by the inverse of the square of the error.

## 6 SO<sub>2</sub> - HCL RATIO

To compare the HCl-emission estimation of Popocatépetl of this work to other estimations about the emission of Popocatépetl we calculate the SO<sub>2</sub> emissions using the average SO<sub>2</sub>/HCl ratio, because there are much more SO<sub>2</sub> measurements than HCl measurements. The ratio between SO<sub>2</sub> and HCl is reported by Taquet et al. (2019) using the NDACC-filter 3 which covers the spectral range around 2500 cm<sup>-1</sup> and at 2800<sup>-1</sup>. However this work is just based on measurements in the near infra-red spectral region and the HCl columns are retrieved from the 1<sup>st</sup> overtone, which results in a slightly different column than HCl retrieval from the fundamental band (Taquet et al., 2019). Therefore the HCl/SO<sub>2</sub> weight ratio of 0.084 from the retrieval of the 1st overtone band of HCl and the SO<sub>2</sub> retrieval from the other spectral regions. The spectral regions of the SO<sub>2</sub> and HCl-1<sup>st</sup>-overtone retrieval are covered by different bandpass filters and cannot be measured simultaneously, therefore the correlation suffer from the limited coincidences, but using the same HCl to estimate the SO<sub>2</sub> ratios and the HCl flux retrieval eliminate the error from the HCl-spectroscopic inconsistency. Never the less the ratio SO<sub>2</sub>/HCl of this work should be used carefully if compared to other studies of the plume composition. The error in flux estimation is dominated by the estimation of wind speed, direction and resulting geometry, and not too much by the quality of the retrieval products. The calculation of the ratio SO<sub>2</sub>/HCl in this work is a very rough estimation and simplified. Taquet et al. (2019) determined the correlation from both HCl-products and the ratio between HCl-fundamental band and SO<sub>2</sub> focusing on the geophysical variation and time series of this ratio and should be consulted if the ratio is needed for geophysical interpretation.

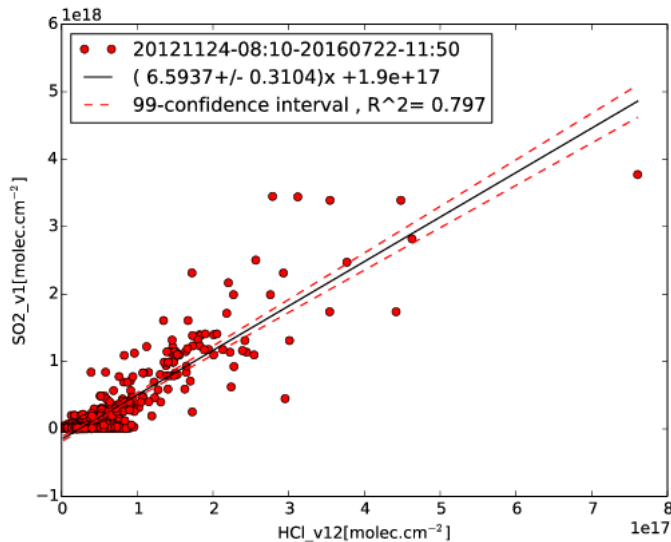


**Figure S24.** Overall average ratio between SO<sub>2</sub> and HCl columns. The HCl column is retrieved from the 1<sup>st</sup> overtone in the NIR infrared. The correlation is done with consecutive measurements which are taken in between few minutes. The ratio corresponds to a HCl/SO<sub>2</sub> weight ratio of 0.084.

## 7 HCL FLUX MEASUREMENTS

The emission estimation of volcanic HCl from a single event depends on the measurements of the vertical column, the solar zenith angle and wind data from the NARR-reanalysis data, as described in the main text of the article. The measurements on which the flux calculation is based is rather simple, and uses directly the columns reconverted to the slant columns. However the model data and estimated plume height (6000m.a.s.l) might be off and allow for a check of consistency. For the quality assurance, we consider more quantities as the duration of the plume, the distance from the observation site to the plume and even calculate more quantities as the concentration and plume-width, assuming a homogeneous plume with circular cross-section. These parameters are graphically shown as histograms in Figure S26 and described in the figure caption. Quality control might introduce statistical bias and we consider the histograms of the most important parameters. The trade off in the quality control aims to use most available data, but to identify clearly erroneous data and exclude some of them carefully without bias the average asymmetrically.

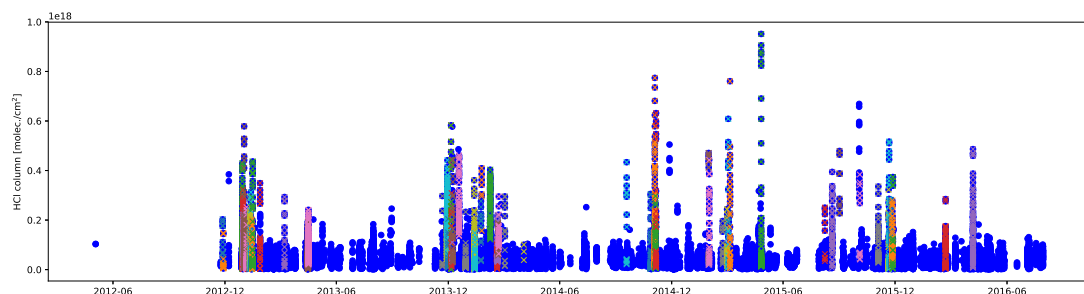


**Figure S25.** HCl vertical columns measured in Altzomoni are showed as blue dots. The different days which have been used for reconstruction of the daily volcanic flux, are marked differently.

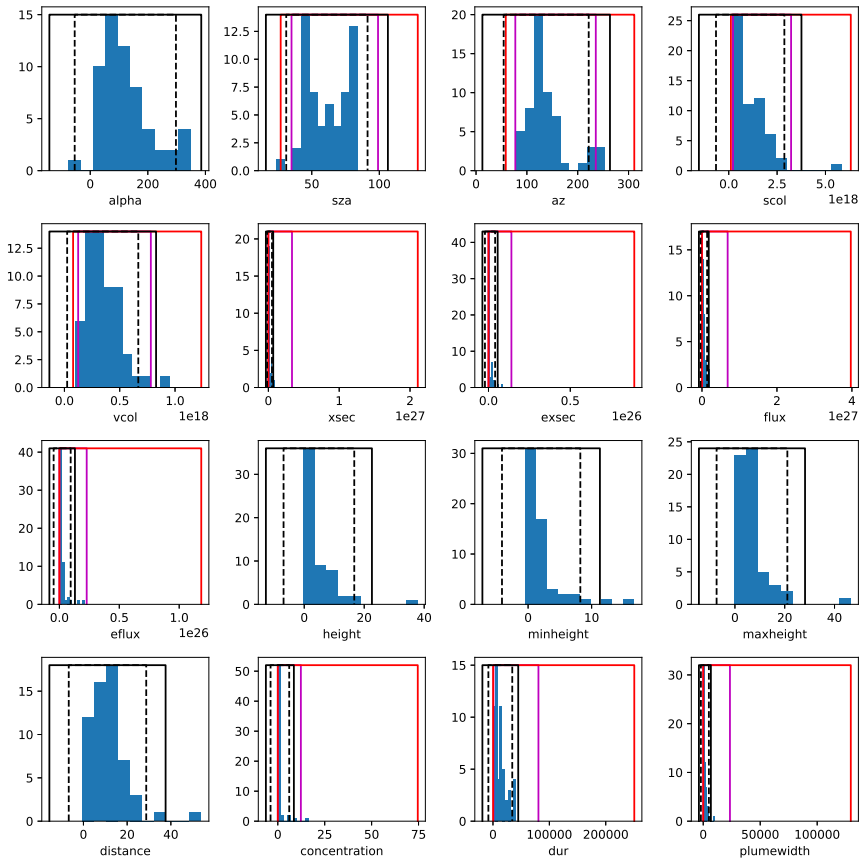


**Figure S26.** Histograms for parameters calculated or used for the HCl flux estimation of 65 events. The quality control identified 7 events as erroneous, as the geometrical quantities as height, or distance are unrealistic. To get an impression how selection might impact an average the 65% and 95% interval in the histograms of the used, measured or reconstructed parameters of the set of events are marked with black dashed and solid lines assuming a Gaussian distribution as well as magenta and red assuming a log-normal distribution for parameter which are positive. The 16 parameters are the angle of the propagation of the plume with the cross section, the solar zenith angle, the aolar azimuth angle, the maximal slant column of HCl in [cm<sup>-1</sup>], the maximal maximal vertical column of HCl in [cm<sup>-1</sup>], the integrated plume cross-section [molec./m], the error in this plume cross-section (based on the total error of the PROFFIT retrieval, which is analytically calculated), the finally calculated flux and the error in it. the estimated average, minimal and maximal height of the plume [km]. The distance between observer site and plume, the concentration of the plume assuming a circular plume [ppm], the duration [s] of the plume event and the plume width [m](assuming a circular plume).

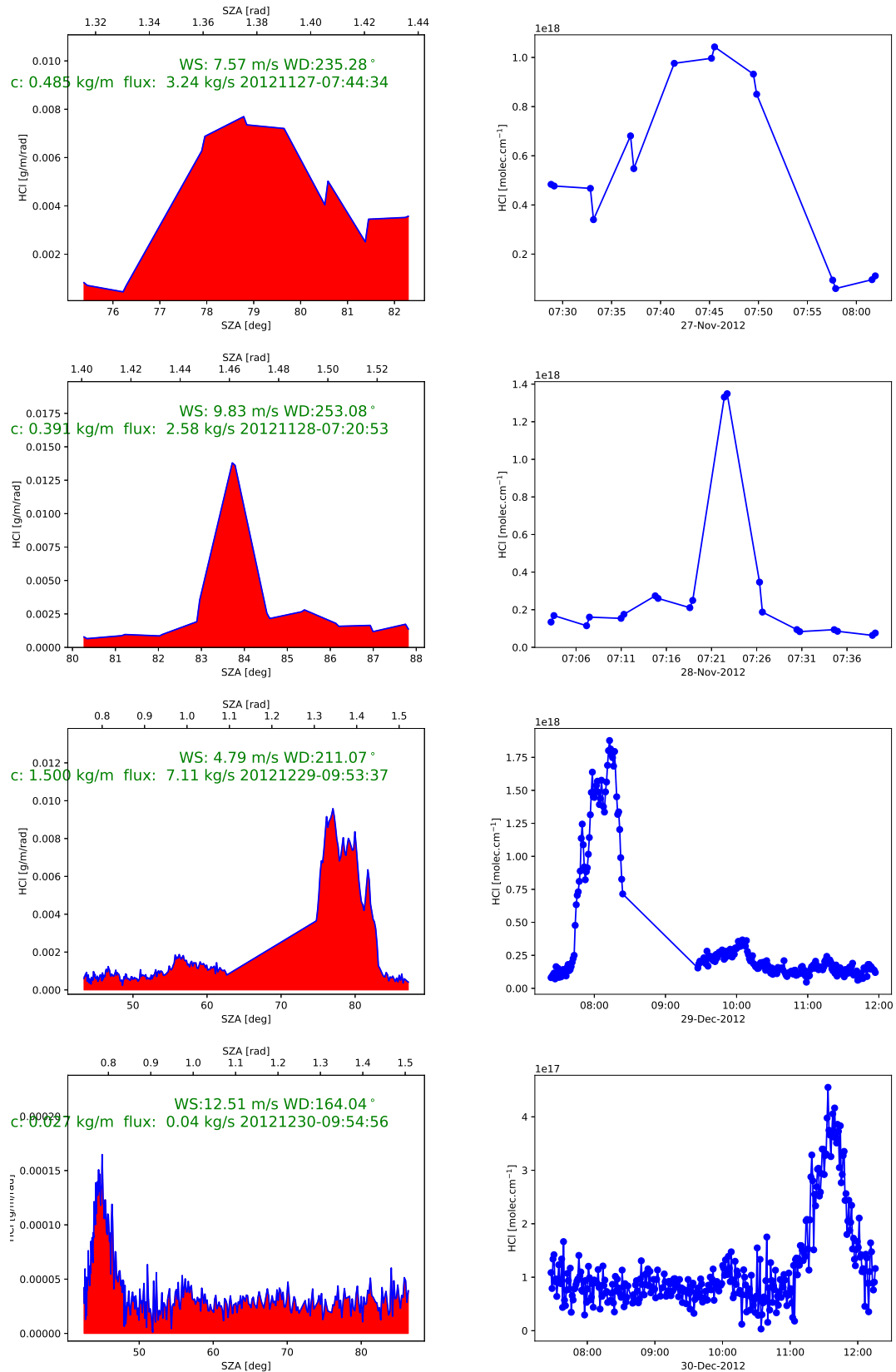
Date-Time	HCl Flux [molec.s <sup>-1</sup> ]	HCl Flux [kg s <sup>-1</sup> ]	SO <sub>2</sub> Flux [kg s <sup>-1</sup> ]	WD	WS	Distance	height	$\alpha$	plume width & concentration
20121127-07:44:34	5.36e+25 ± 3.11e+24	3.24 ± 0.19	37.63 ± 2.77	235.28	7.57	12.19	2.32	61.98	350.33
20121127-07:44:34	5.36e+25 ± 3.11e+24	3.24 ± 0.19	37.63 ± 2.77	235.28	7.57	12.19	2.32	61.98	350.33
20121128-07:20:53	4.26e+25 ± 2.37e+24	2.58 ± 0.14	29.90 ± 2.15	253.08	9.83	16.89	1.84	42.17	465.34
20121229-09:53:37	1.17e+26 ± 2.63e+24	7.11 ± 0.16	82.45 ± 4.18	211.07	4.79	8.43	3.15	98.27	1889.79
20121230-09:54:56	6.42e+23 ± 1.28e+22	0.04 ± 0.00	0.45 ± 0.02	164.04	12.51	0.60	0.41	173.50	139.17
20121231-09:33:17	7.41e+25 ± 1.44e+24	4.49 ± 0.09	52.03 ± 2.57	171.98	14.61	2.73	1.38	143.34	628.64
20130101-09:41:41	7.17e+25 ± 7.65e+23	4.34 ± 0.05	50.36 ± 2.35	194.51	9.74	6.52	3.09	116.97	732.16
20130105-08:17:41	8.99e+25 ± 1.41e+24	5.45 ± 0.09	63.15 ± 3.04	238.30	10.79	12.70	1.96	59.45	939.17
20130110-07:56:15	8.48e+25 ± 1.06e+24	5.14 ± 0.06	59.57 ± 2.81	235.09	8.32	12.03	2.48	63.34	609.46
20130111-08:05:32	7.81e+25 ± 6.18e+23	4.73 ± 0.04	54.84 ± 2.53	261.53	3.80	20.09	2.15	34.00	1091.15
20130112-08:03:34	5.93e+25 ± 1.77e+24	3.59 ± 0.11	41.63 ± 2.27	258.52	7.08	18.11	3.15	38.61	1041.59
20130113-08:01:34	5.80e+25 ± 9.19e+23	3.51 ± 0.06	40.71 ± 1.96	245.38	8.16	14.61	1.80	50.18	614.30
20130114-08:22:01	6.90e+25 ± 1.25e+24	4.17 ± 0.08	48.42 ± 2.37	238.09	6.53	12.76	2.25	58.84	1271.44
20130115-09:01:03	2.68e+25 ± 3.09e+23	1.62 ± 0.02	18.81 ± 0.88	200.12	4.51	6.83	1.89	99.56	404.08
<b>20130127-10:19:46</b>	<b>1.82e+25 ± 1.25e+24</b>	<b>1.10 ± 0.08</b>	<b>12.75 ± 1.05</b>	<b>141.79</b>	<b>1.97</b>	<b>-122.52</b>	<b>-78.68</b>	<b>178.02</b>	<b>33820.02</b>
20130308-07:56:40	7.25e+25 ± 2.26e+24	4.39 ± 0.14	50.94 ± 2.81	209.41	4.68	8.52	2.61	72.27	753.64
20130415-12:06:57	5.23e+25 ± 9.08e+23	3.17 ± 0.06	36.71 ± 1.79	187.06	7.57	6.91	6.31	139.41	2397.95
20130416-08:28:15	6.13e+25 ± 8.67e+23	3.71 ± 0.05	43.04 ± 2.05	214.98	5.04	10.54	6.41	57.04	2208.01
20131121-07:54:58	2.76e+25 ± 1.29e+24	1.67 ± 0.08	19.40 ± 1.27	205.46	4.19	7.55	1.61	91.04	278.82
20131128-09:19:00	7.63e+25 ± 1.54e+24	4.62 ± 0.09	53.57 ± 2.66	226.53	3.17	10.15	4.67	83.68	2020.23
20131129-14:39:51	1.58e+25 ± 1.20e+23	0.95 ± 0.01	11.06 ± 0.51	149.32	1.74	3.11	1.89	244.93	624.50
<b>20131130-16:28:59</b>	<b>5.45e+24 ± 1.74e+23</b>	<b>0.33 ± 0.01</b>	<b>3.83 ± 0.21</b>	<b>50.46</b>	<b>2.53</b>	<b>-62.22</b>	<b>-16.00</b>	<b>369.64</b>	<b>2091.13</b>
20131205-10:50:22	1.21e+24 ± 5.04e+22	0.07 ± 0.00	0.85 ± 0.05	164.16	3.63	0.33	0.21	164.12	71.71
20131206-12:06:20	3.56e+25 ± 4.44e+24	2.16 ± 0.27	25.01 ± 3.32	151.21	9.20	10.86	7.35	193.05	2860.39
20131207-09:11:27	2.23e+23 ± 3.10e+22	0.01 ± 0.00	0.16 ± 0.02	171.76	7.25	2.35	1.06	137.48	11.42
20131208-09:37:38	6.47e+25 ± 1.92e+24	3.92 ± 0.12	45.43 ± 2.47	187.29	6.15	5.29	2.07	120.86	733.14
20131218-11:47:44	7.34e+24 ± 9.01e+22	0.44 ± 0.01	5.15 ± 0.24	126.78	3.86	10.46	7.55	220.65	272.06
20131229-08:27:41	1.28e+26 ± 9.59e+24	7.77 ± 0.58	90.07 ± 7.88	233.31	18.19	11.44	2.82	68.28	1386.37
20140112-12:43:09	5.91e+25 ± 8.10e+23	3.58 ± 0.05	41.52 ± 1.97	180.42	8.24	4.90	2.29	138.28	1157.99
20140113-08:45:51	5.40e+25 ± 1.35e+24	3.27 ± 0.08	37.92 ± 1.97	226.86	11.35	10.59	2.58	72.81	1398.50
20140123-09:36:54	2.60e+25 ± 1.39e+24	1.57 ± 0.08	18.27 ± 1.28	63.43	0.83	11.91	6.61	249.53	2567.03
20140124-11:20:00	4.87e+24 ± 6.08e+23	0.29 ± 0.04	3.42 ± 0.45	208.63	1.98	9.08	6.39	118.11	284.27
20140207-10:45:09	7.44e+24 ± 7.79e+22	0.45 ± 0.00	5.22 ± 0.24	236.47	1.00	10.98	7.66	80.48	603.04
20140218-12:53:26	3.07e+25 ± 2.86e+24	1.86 ± 0.17	21.58 ± 2.24	13.74	3.28	7.98	5.43	314.67	2497.71
20140219-13:16:21	9.76e+24 ± 6.88e+23	0.59 ± 0.04	6.85 ± 0.57	53.33	0.59	53.90	37.86	348.63	9798.23
<b>20140220-08:46:16</b>	<b>2.19e+25 ± 2.06e+24</b>	<b>1.32 ± 0.12</b>	<b>15.35 ± 1.61</b>	<b>289.46</b>	<b>3.54</b>	<b>-731.68</b>	<b>-221.64</b>	<b>-0.72</b>	<b>74202.96</b>

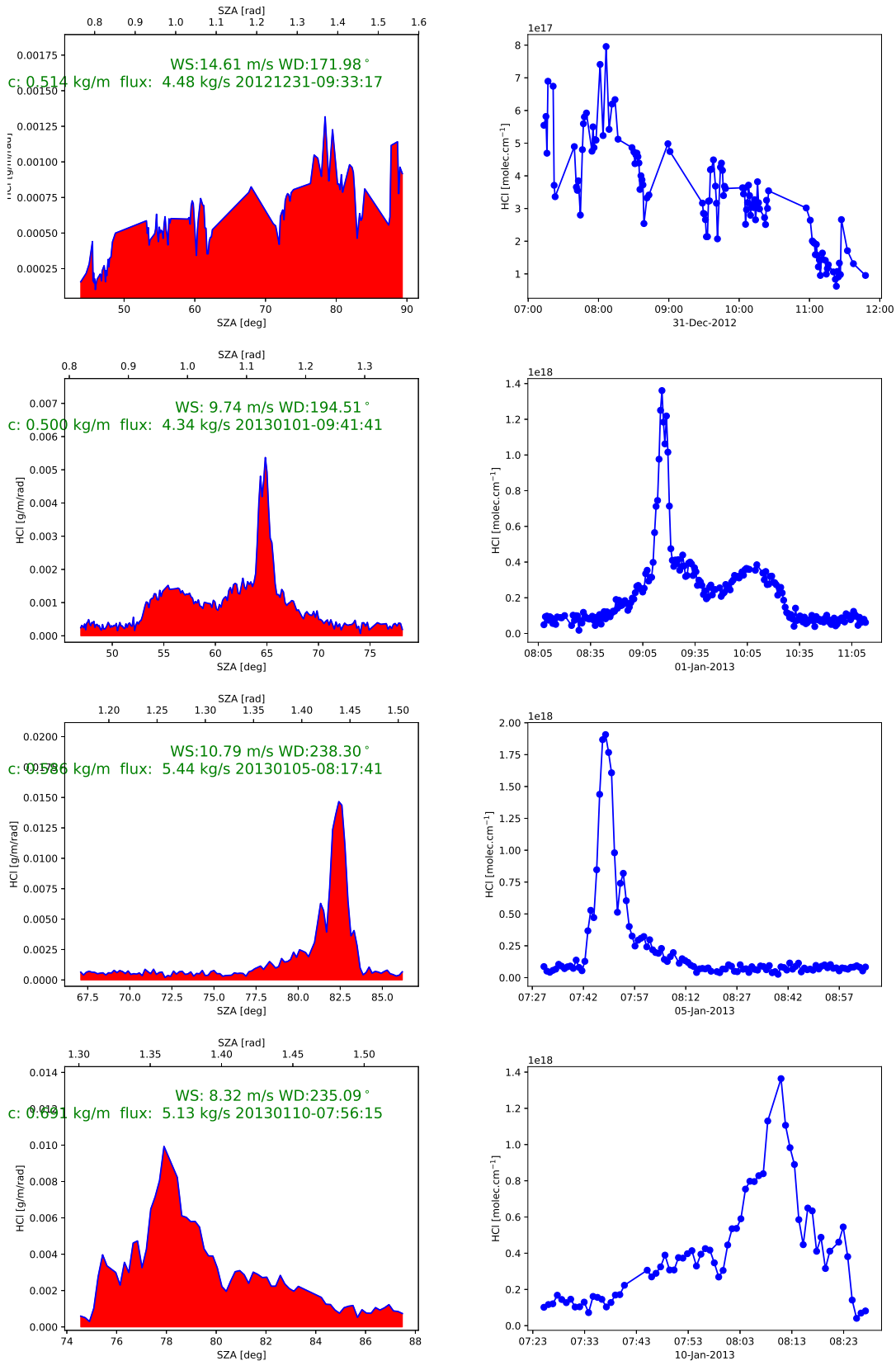
Date-Time	HCl Flux [molec.s <sup>-1</sup> ]	HCl Flux [kg s <sup>-1</sup> ]	HCl Flux [kg s <sup>-1</sup> ]	SO <sub>2</sub> Flux [kg s <sup>-1</sup> ]	WD	WS	Distance	height	$\alpha$	plume width & concentration
20140221-10:22:04	1.74e+25 ± 1.27e+24	1.05 ± 0.08	12.21 ± 1.05	185.47	3.36	5.33	3.76	127.93	1274.34	0.10
<b>20140303-09:25:45</b>	<b>1.75e+25 ± 1.28e+24</b>	<b>1.06 ± 0.08</b>	<b>12.30 ± 1.06</b>	<b>155.09</b>	<b>4.65</b>	<b>-2.93</b>	<b>-1.95</b>	<b>144.59</b>	<b>590.52</b>	<b>0.44</b>
20140403-09:08:23	9.66e+23 ± 1.81e+23	0.06 ± 0.01	0.68 ± 0.13	231.29	8.14	14.42	8.74	46.65	40.43	2.36
20140918-08:14:07	3.27e+24 ± 1.76e+23	0.20 ± 0.01	2.30 ± 0.16	162.29	3.52	-0.36	-0.26	128.46	69.07	5.90
20141027-17:12:24	4.38e+25 ± 5.28e+23	2.65 ± 0.03	30.77 ± 1.45	104.48	4.36	18.78	2.59	328.75	886.68	0.58
<b>20141103-10:01:55</b>	<b>8.14e+24 ± 9.47e+22</b>	<b>0.49 ± 0.01</b>	<b>5.72 ± 0.27</b>	<b>157.02</b>	<b>5.15</b>	<b>-11.59</b>	<b>-8.88</b>	<b>173.46</b>	<b>1971.36</b>	<b>0.08</b>
<b>20141104-16:29:04</b>	<b>5.35e+22 ± 2.54e+21</b>	<b>0.00 ± 0.00</b>	<b>0.04 ± 0.00</b>	<b>163.78</b>	<b>4.51</b>	<b>-0.02</b>	<b>-0.01</b>	<b>257.17</b>	<b>1.50</b>	<b>127.32</b>
20141105-10:19:19	1.56e+25 ± 1.43e+24	0.94 ± 0.09	10.93 ± 1.12	168.38	8.04	13.15	10.41	175.96	4346.59	0.03
20150130-12:17:23	4.03e+25 ± 3.26e+24	2.44 ± 0.20	28.33 ± 2.63	319.89	3.82	21.99	16.32	12.02	4912.96	0.05
20150130-11:56:16	2.88e+25 ± 1.89e+24	1.74 ± 0.11	20.19 ± 1.61	319.89	3.82	23.95	17.89	11.02	1498.18	0.42
20150131-08:14:53	9.06e+25 ± 3.01e+24	5.48 ± 0.18	63.59 ± 3.58	242.89	5.66	14.56	2.74	49.93	615.86	1.30
20150222-10:58:09	1.11e+26 ± 2.08e+25	6.73 ± 1.26	78.06 ± 15.01	99.66	5.72	24.99	14.81	204.07	6296.25	0.03
20150301-15:32:13	5.97e+25 ± 3.66e+24	3.62 ± 0.22	41.94 ± 3.20	136.27	3.83	5.53	3.04	289.05	1498.73	0.17
20150303-13:42:03	1.18e+26 ± 1.51e+25	7.15 ± 0.91	82.93 ± 11.22	189.81	14.85	5.47	3.88	114.21	926.25	0.24
20150304-08:26:38	2.76e+24 ± 2.18e+23	0.17 ± 0.01	1.94 ± 0.18	181.27	13.51	3.52	1.26	103.77	17.47	16.33
20150306-10:47:22	2.08e+26 ± 8.24e+24	12.60 ± 0.50	146.13 ± 8.81	226.39	3.80	11.22	5.55	63.95	2433.64	0.24
20150426-06:47:37	1.91e+26 ± 1.43e+24	11.54 ± 0.09	133.78 ± 6.16	225.24	6.79	17.93	3.11	33.78	1821.40	0.36
20150808-08:12:52	1.50e+24 ± 6.07e+23	0.09 ± 0.04	1.05 ± 0.43	160.64	8.20	-0.62	-0.31	101.44	81.34	0.67
20150820-06:30:39	4.44e+25 ± 1.56e+24	2.69 ± 0.09	31.16 ± 1.79	191.73	4.51	5.66	1.51	70.19	518.28	0.92
20150901-07:14:13	1.53e+25 ± 6.72e+23	0.93 ± 0.04	10.74 ± 0.68	183.08	1.13	3.77	1.49	86.14	632.81	0.80
20151004-09:13:37	1.16e+23 ± 5.03e+22	0.01 ± 0.00	0.08 ± 0.04	165.59	1.18	0.47	0.31	128.17	53.33	1.04
20151103-16:50:49	2.88e+25 ± 4.51e+23	1.74 ± 0.03	20.21 ± 0.97	120.27	3.47	10.11	1.80	309.56	647.05	0.61
20151120-08:44:50	2.22e+25 ± 2.06e+24	1.34 ± 0.12	15.57 ± 1.61	132.61	3.24	16.55	11.54	200.73	4082.86	0.03
20151121-08:05:09	2.58e+25 ± 1.64e+24	1.56 ± 0.10	18.11 ± 1.41	279.97	1.89	33.69	8.44	17.57	1618.93	0.41
<b>20151124-09:46:09</b>	<b>9.08e+24 ± 6.63e+23</b>	<b>0.55 ± 0.04</b>	<b>6.38 ± 0.55</b>	<b>155.95</b>	<b>4.17</b>	<b>-4.63</b>	<b>-2.76</b>	<b>160.71</b>	<b>355.02</b>	<b>1.24</b>
20151126-15:59:11	4.56e+25 ± 3.17e+24	2.76 ± 0.19	32.02 ± 2.66	140.21	5.08	4.53	2.02	272.83	475.96	0.94
20151127-08:55:52	7.72e+25 ± 7.72e+24	4.68 ± 0.47	54.23 ± 5.96	227.97	3.78	10.63	7.50	106.06	2948.05	0.06
20160221-14:01:22	5.63e+25 ± 3.67e+24	3.41 ± 0.22	39.50 ± 3.14	272.51	1.90	17.37	10.71	141.83	4898.64	0.05
20160406-08:37:20	8.44e+23 ± 7.86e+22	0.05 ± 0.00	0.59 ± 0.06	354.51	0.25	2.21	1.58	-74.27	313.86	0.85
Average	4.94e+25 ± 5.75e+24	2.99 ± 0.35	34.7 ± 4.3							

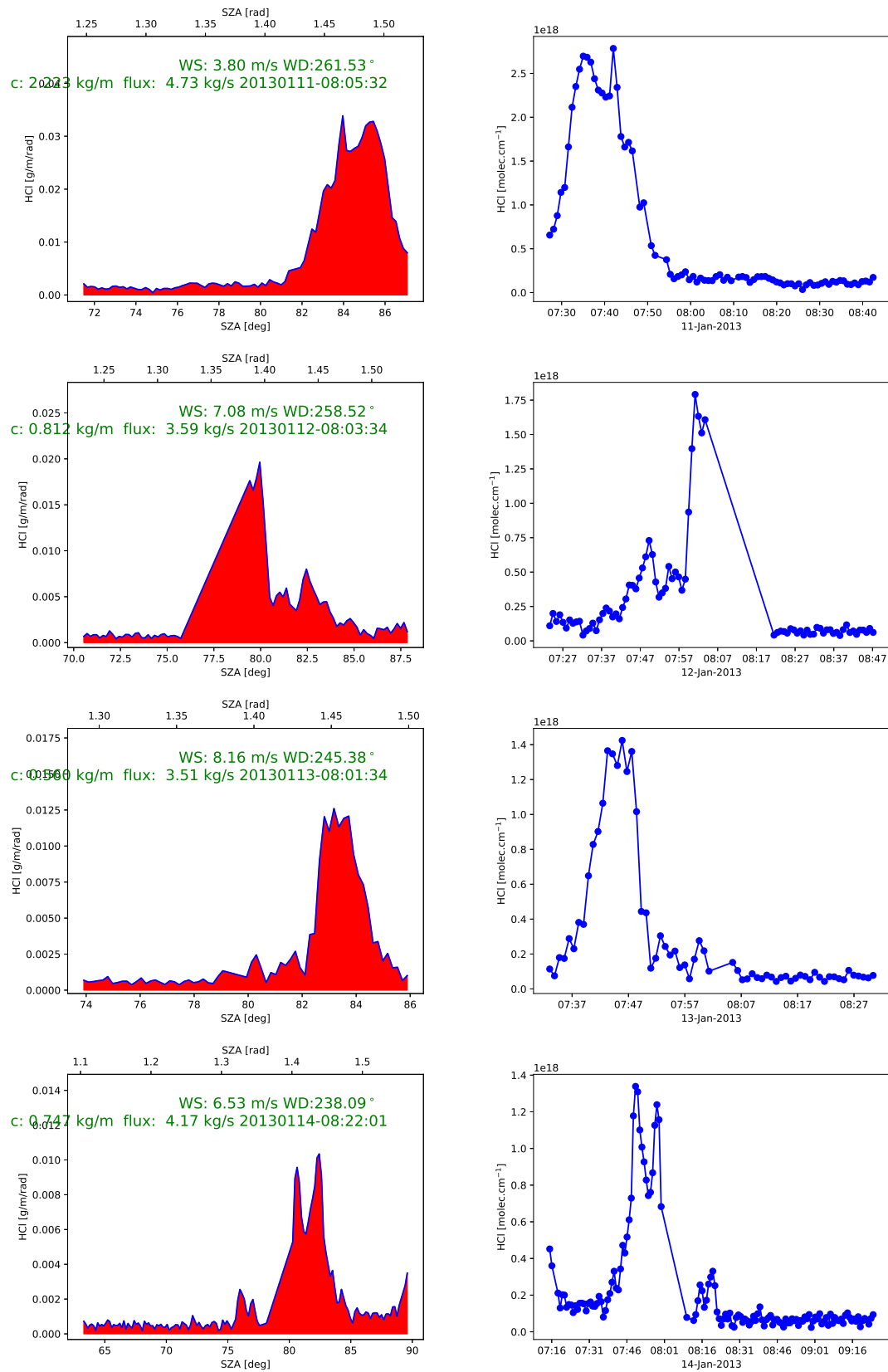
**Table S2.** Events from which the HCl flux was reconstructed. The red marked events have been identified by the quality control as unrealistic results and are excluded from the statistical analysis. The geometrical reconstruction uses the wind direction and speed from the NARR-reanalysis. To estimate a concentration in the plume, the integrated crosssection was divided by the area of a circular crosssection with the plume-width as diameter. The plume-width has been roughly estimated from the solar angles and geometry. The both parameter, concentration and plume-width are only used for the quality control.

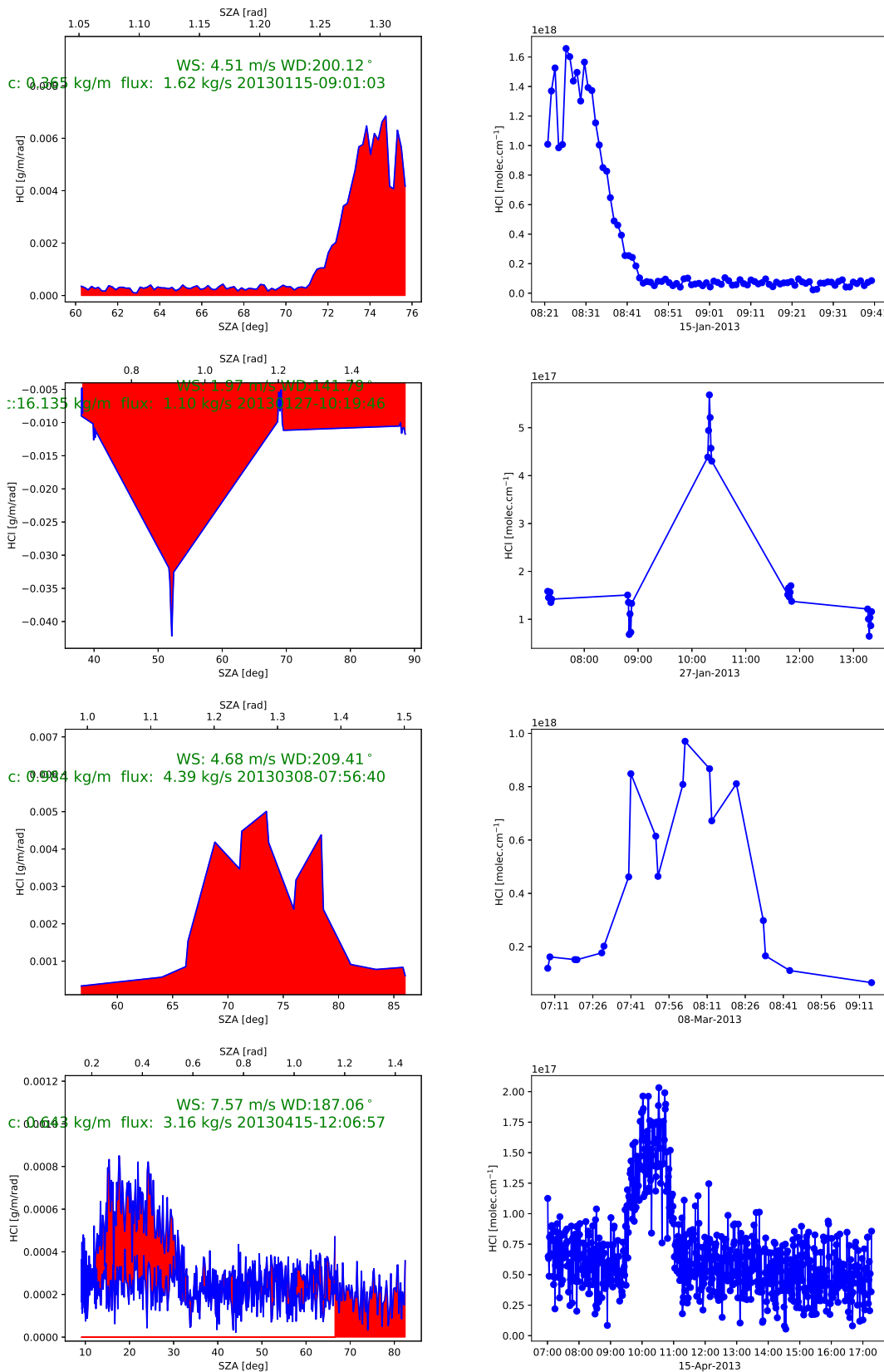
## 7.1 Appendix: Graphics for HCl-flux events:

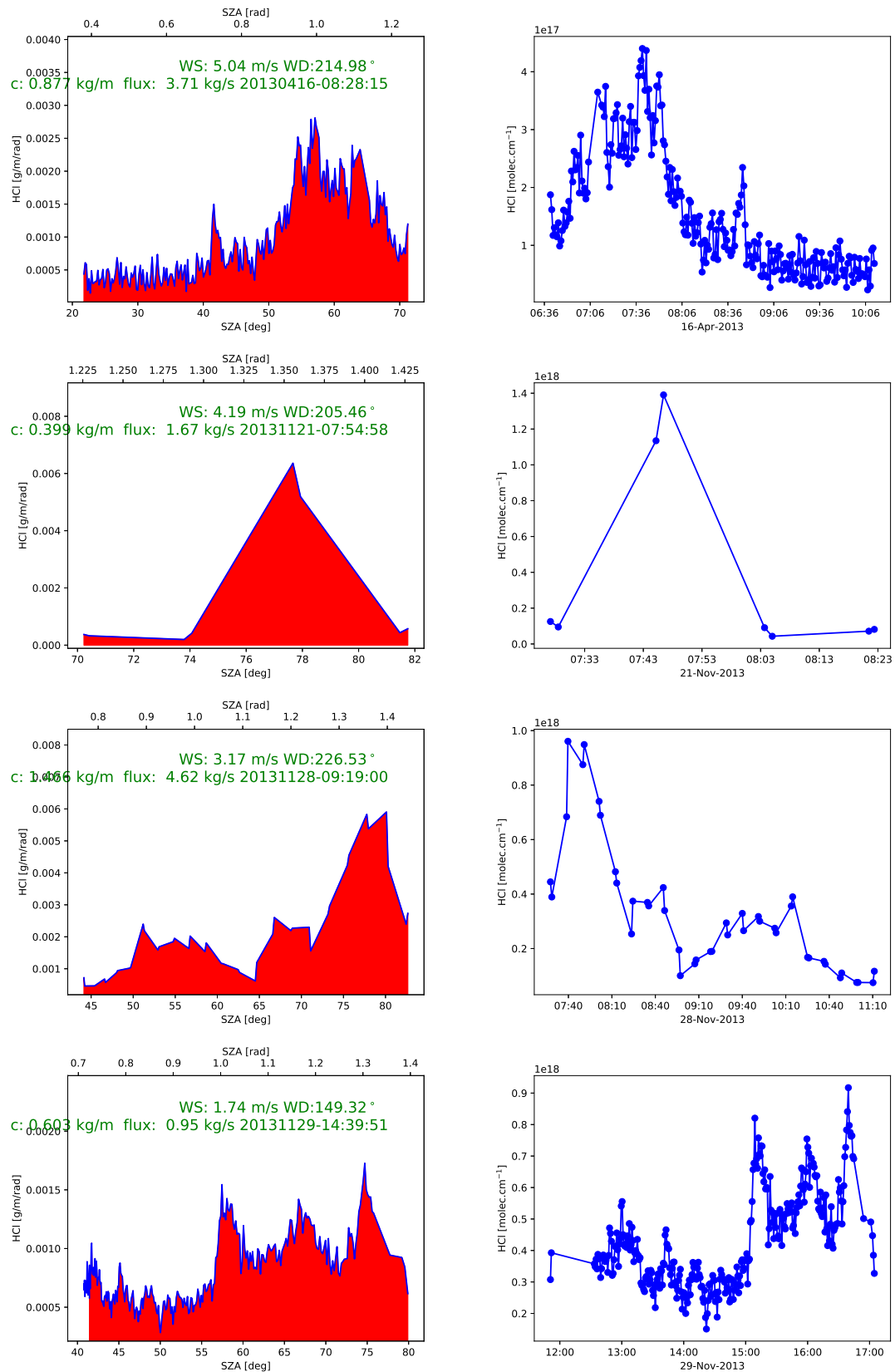
The reconstruction of the volcanic HCl-flux, is detailed explained in the main article. The time series around the volcanic event is manually selected, but the calculation of the flux is then automatically done by a python program, which produce also a set of graphics. In this section we report two plots for each event, which document the time series (right) and the cross-section reconstructed using the NARR-wind direction (left). The differential cross section elements is the outer product of the angle difference between two measurements and the reconstructed distance of the crossing point of the line of sight towards the sun and the plume. Afternoons the difference of the solar zenith angle is negative, but the multiplication with the perpendicular plume propagation velocity will correct for it. However, due to errors in the wind direction, a negative distance and cross section might be calculated as well.

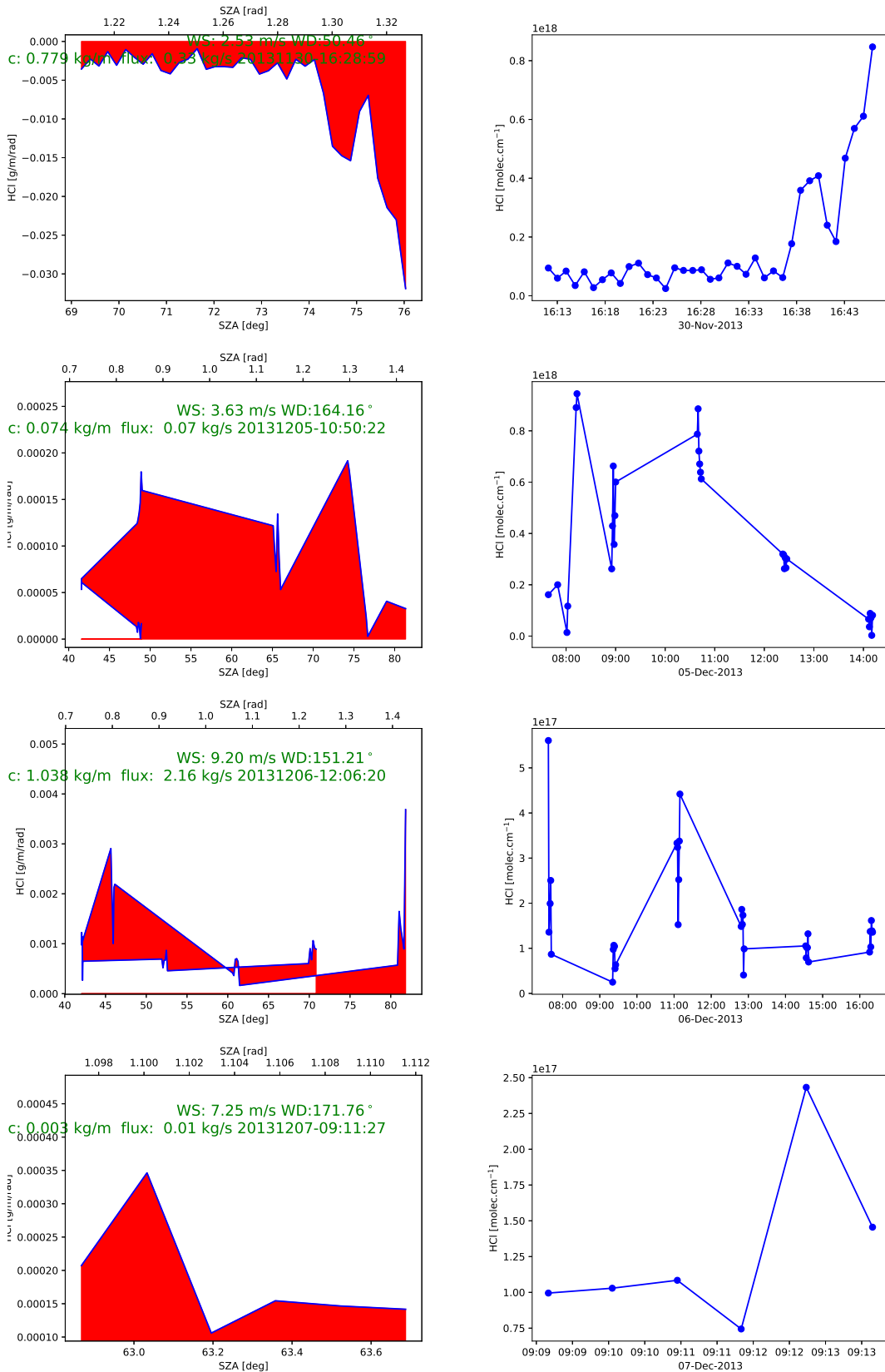


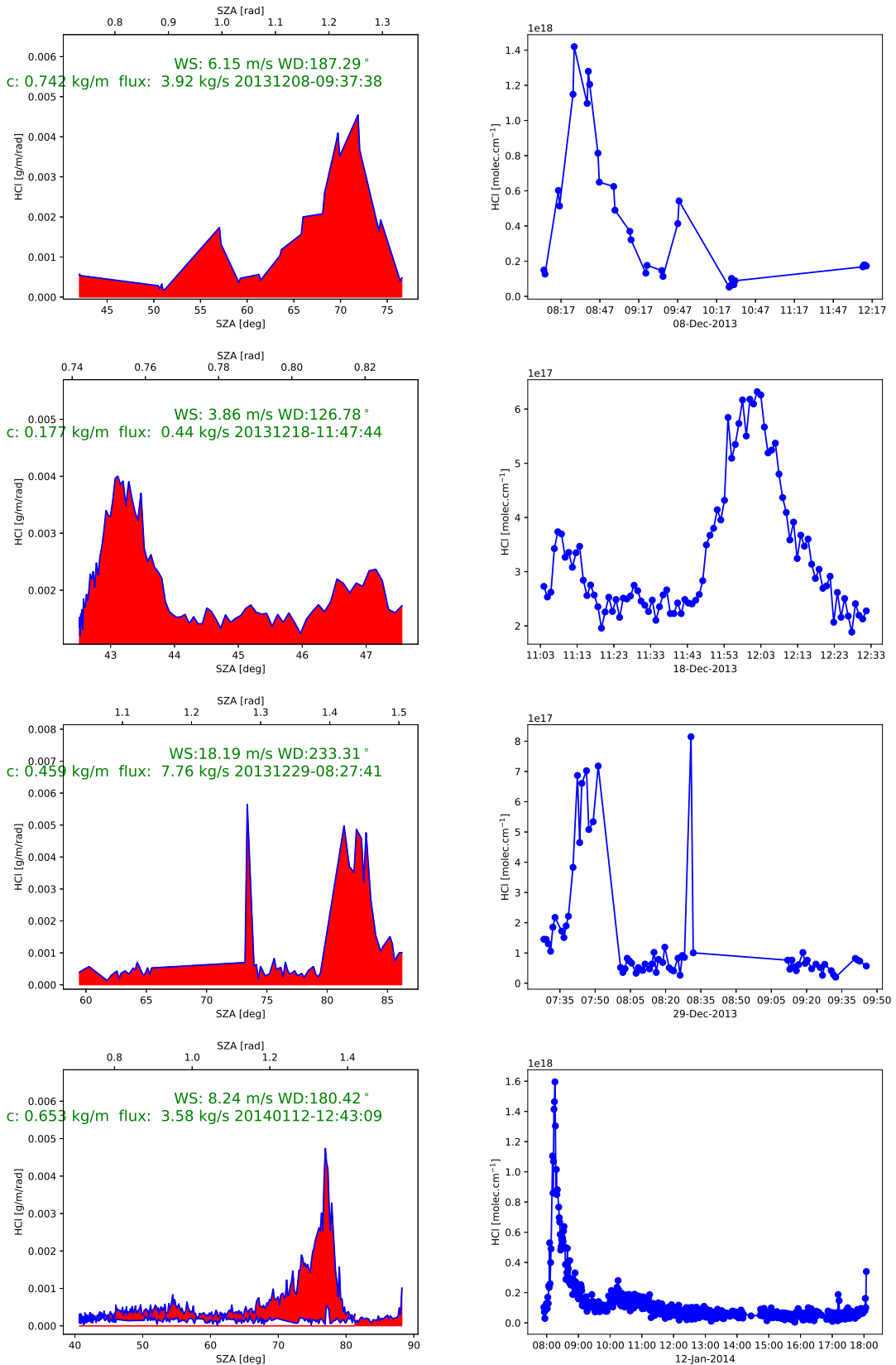


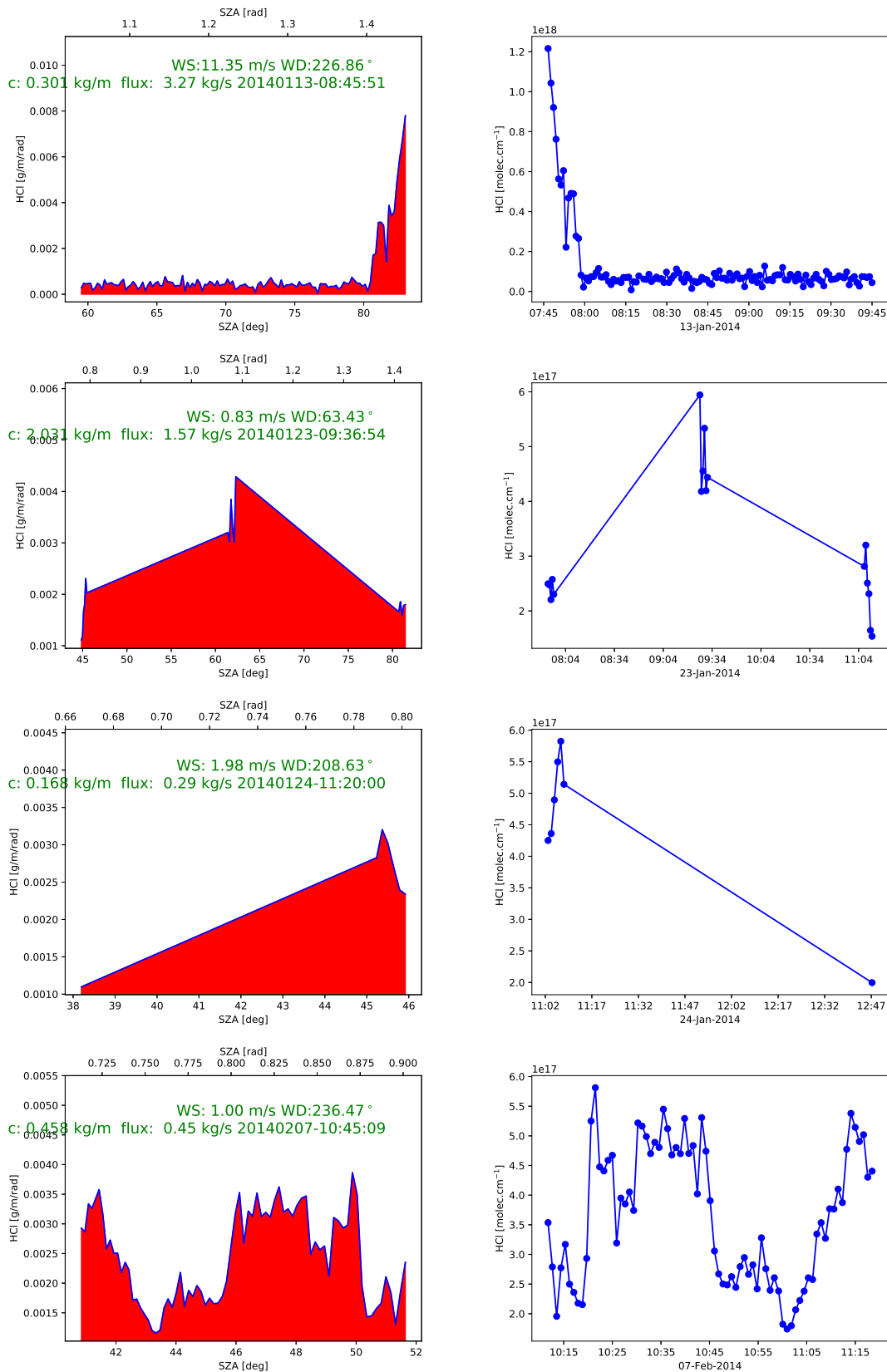


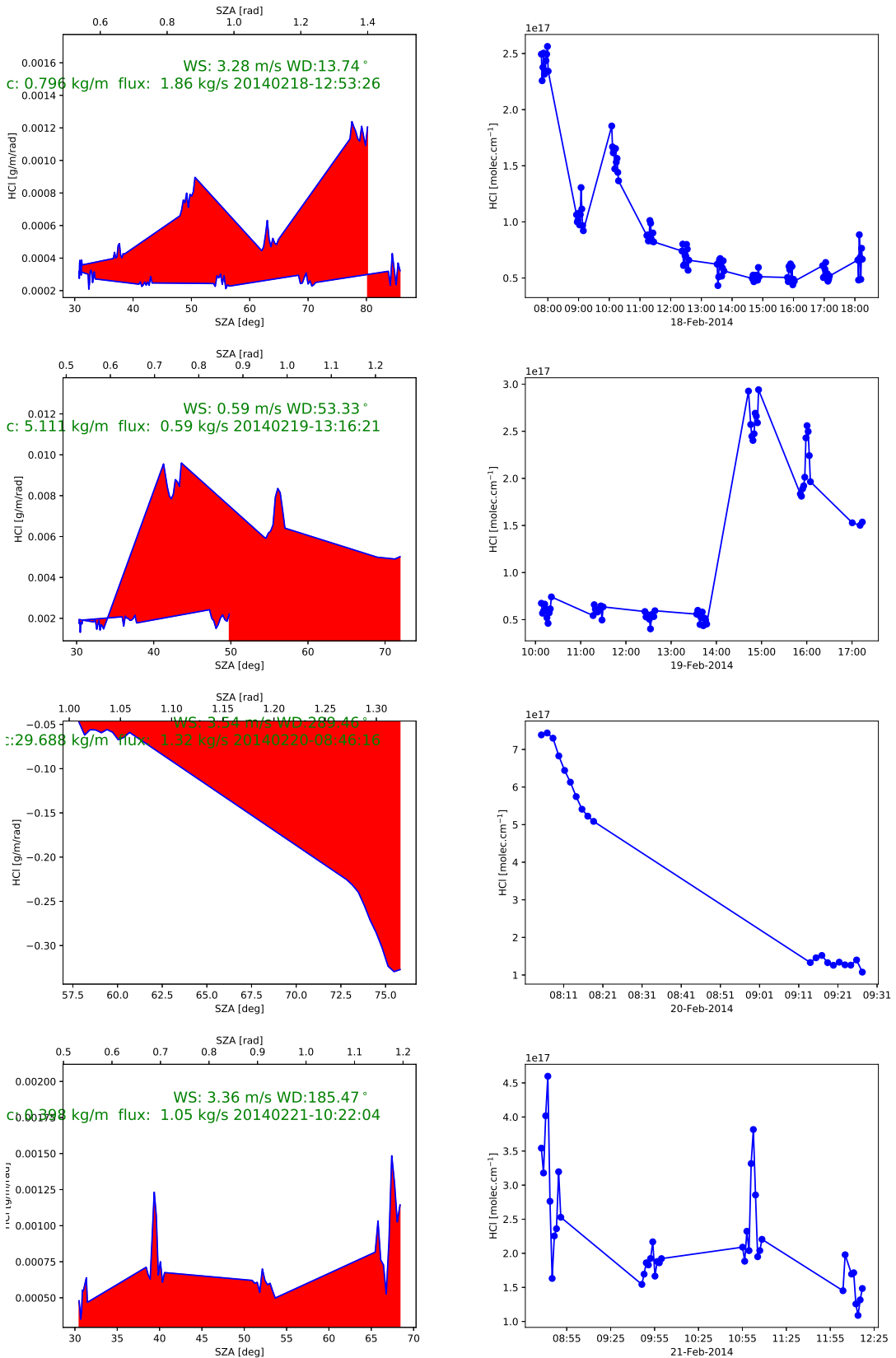


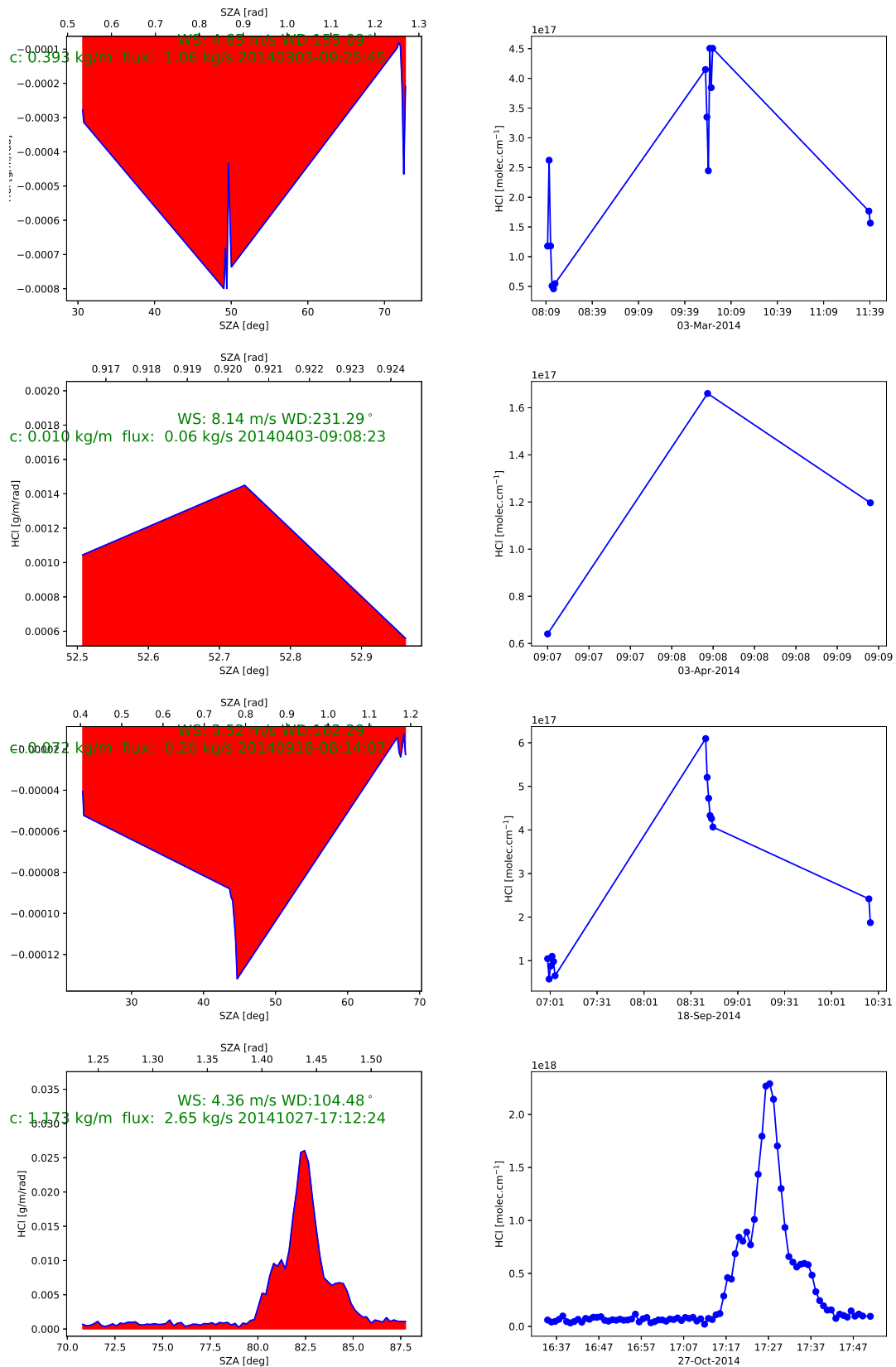


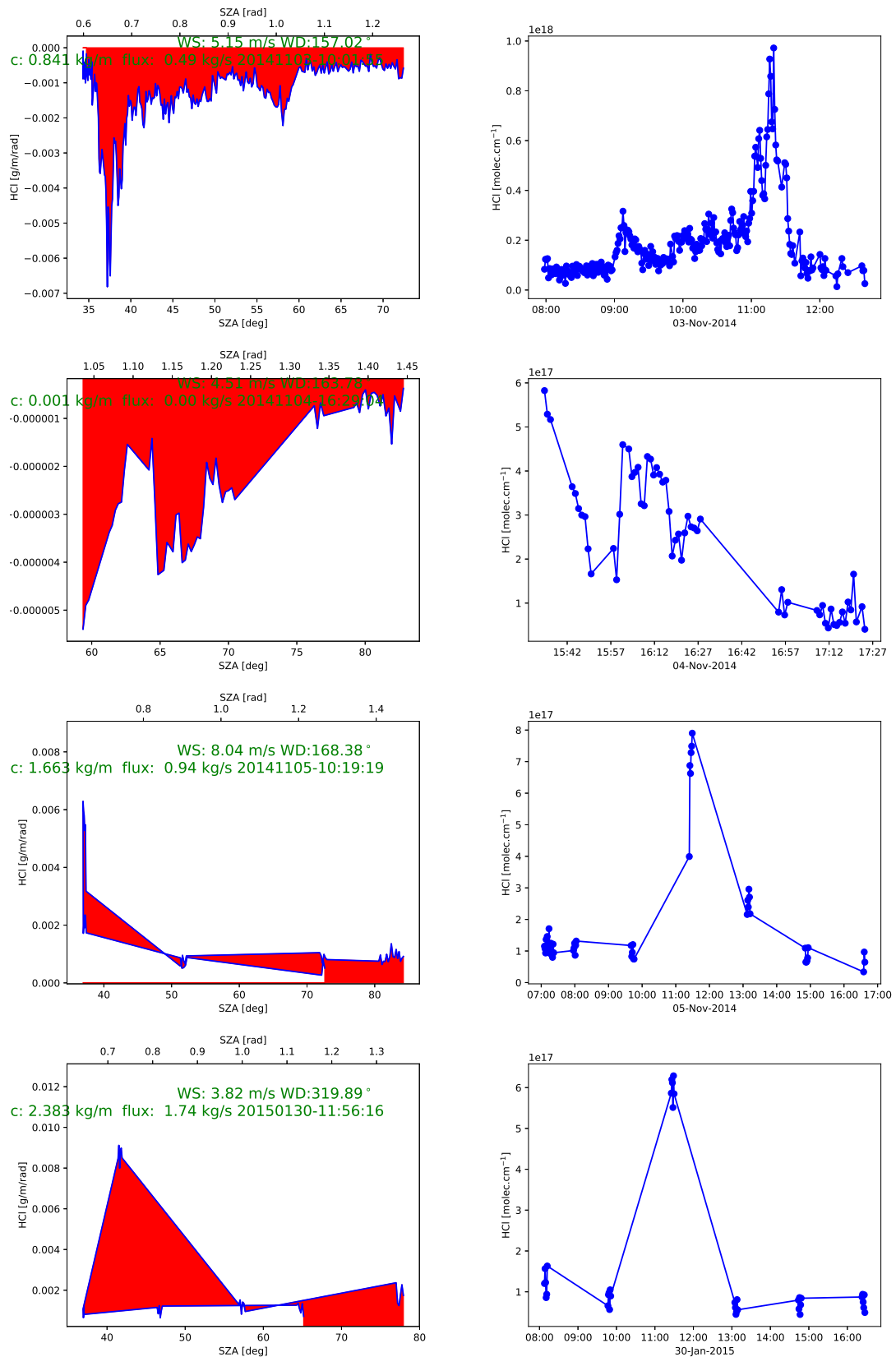


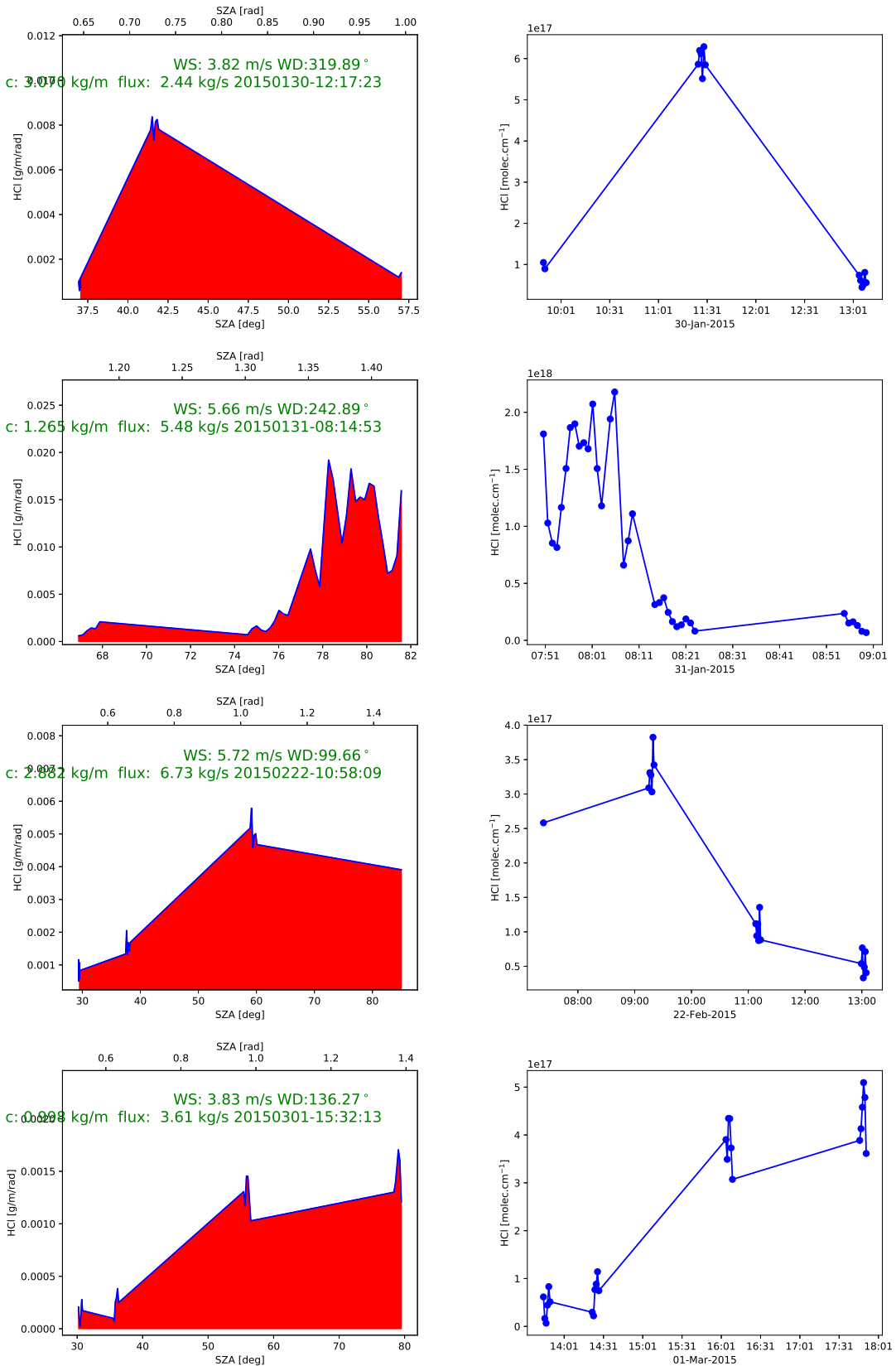


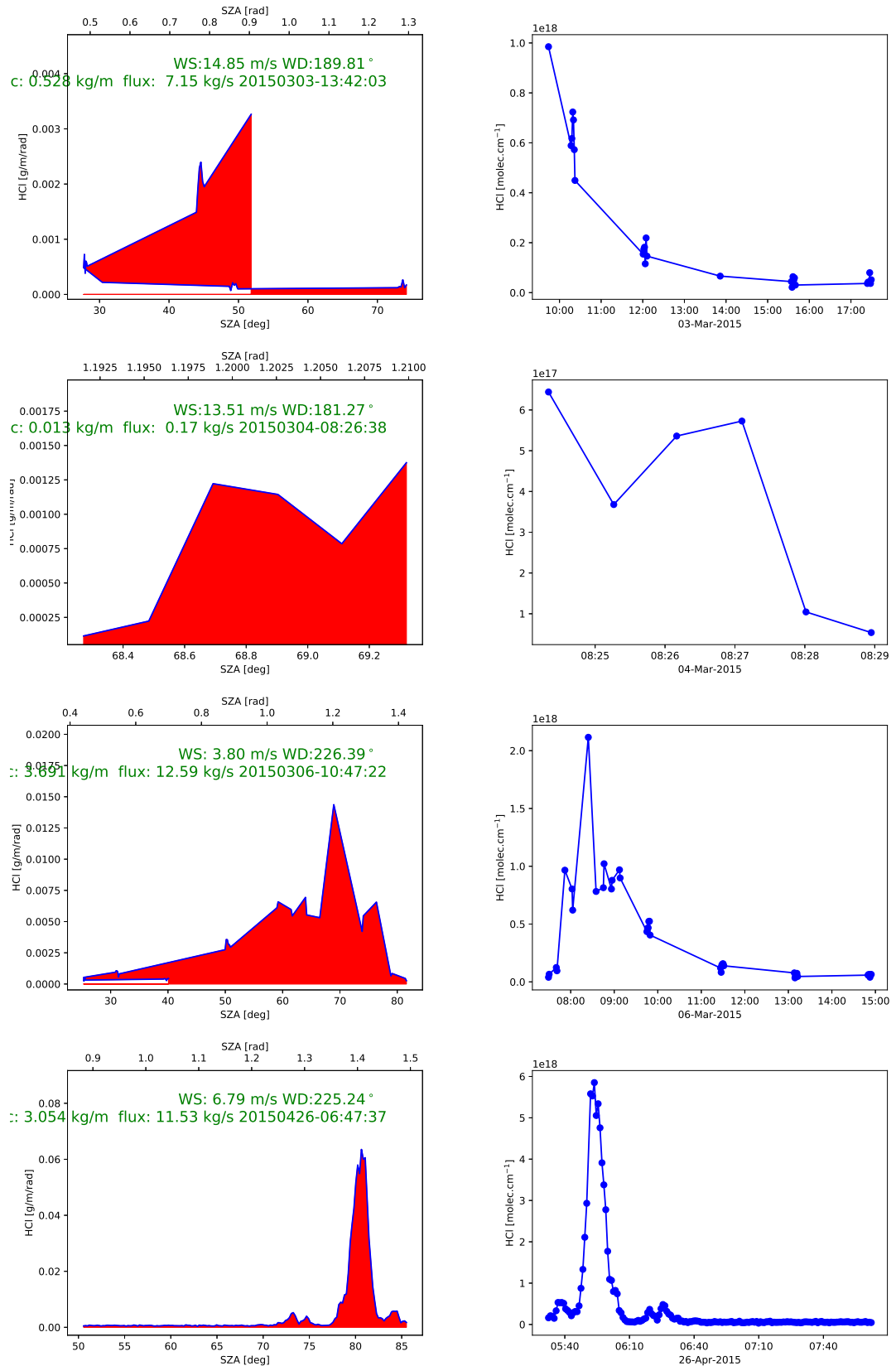


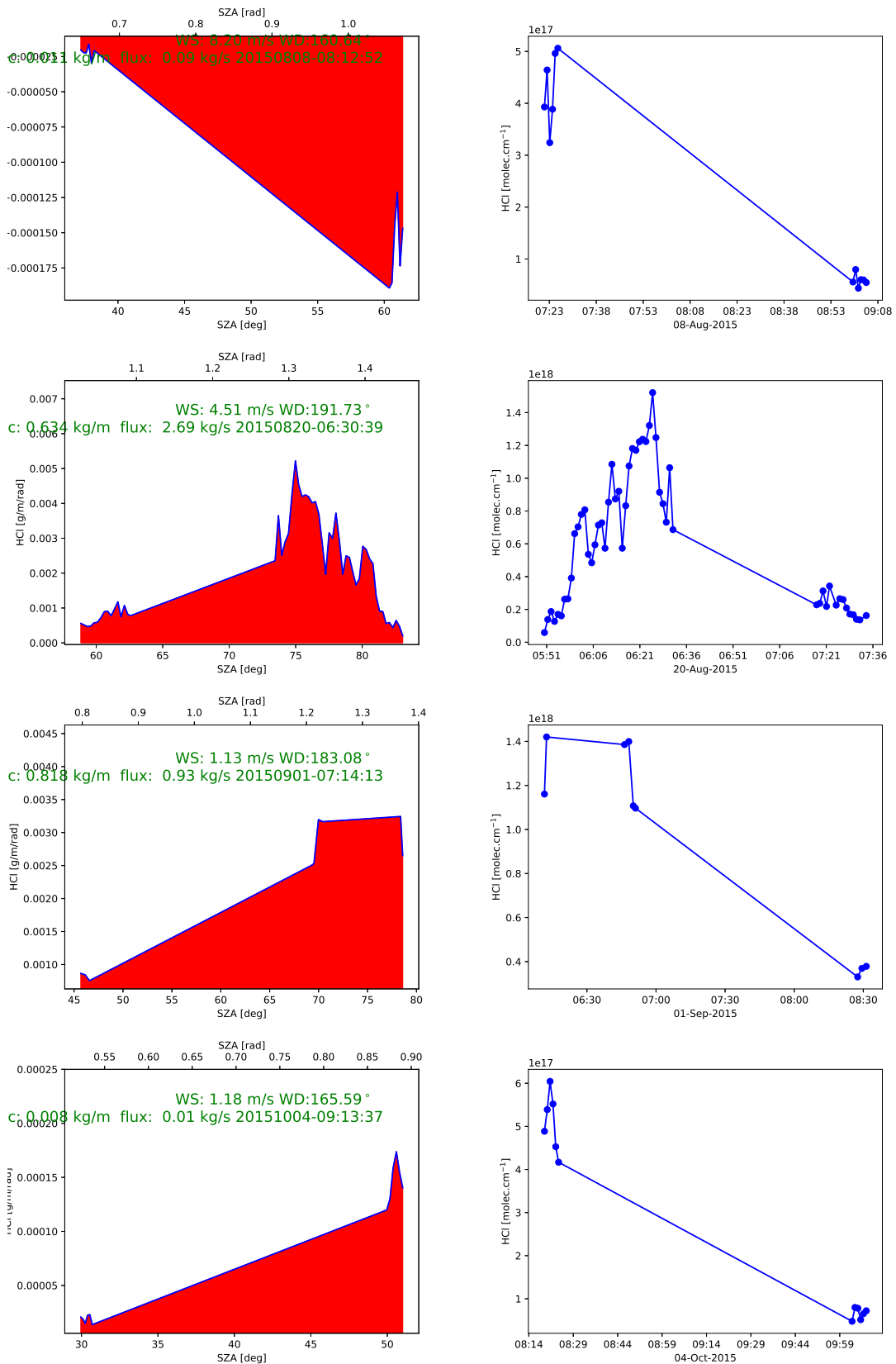


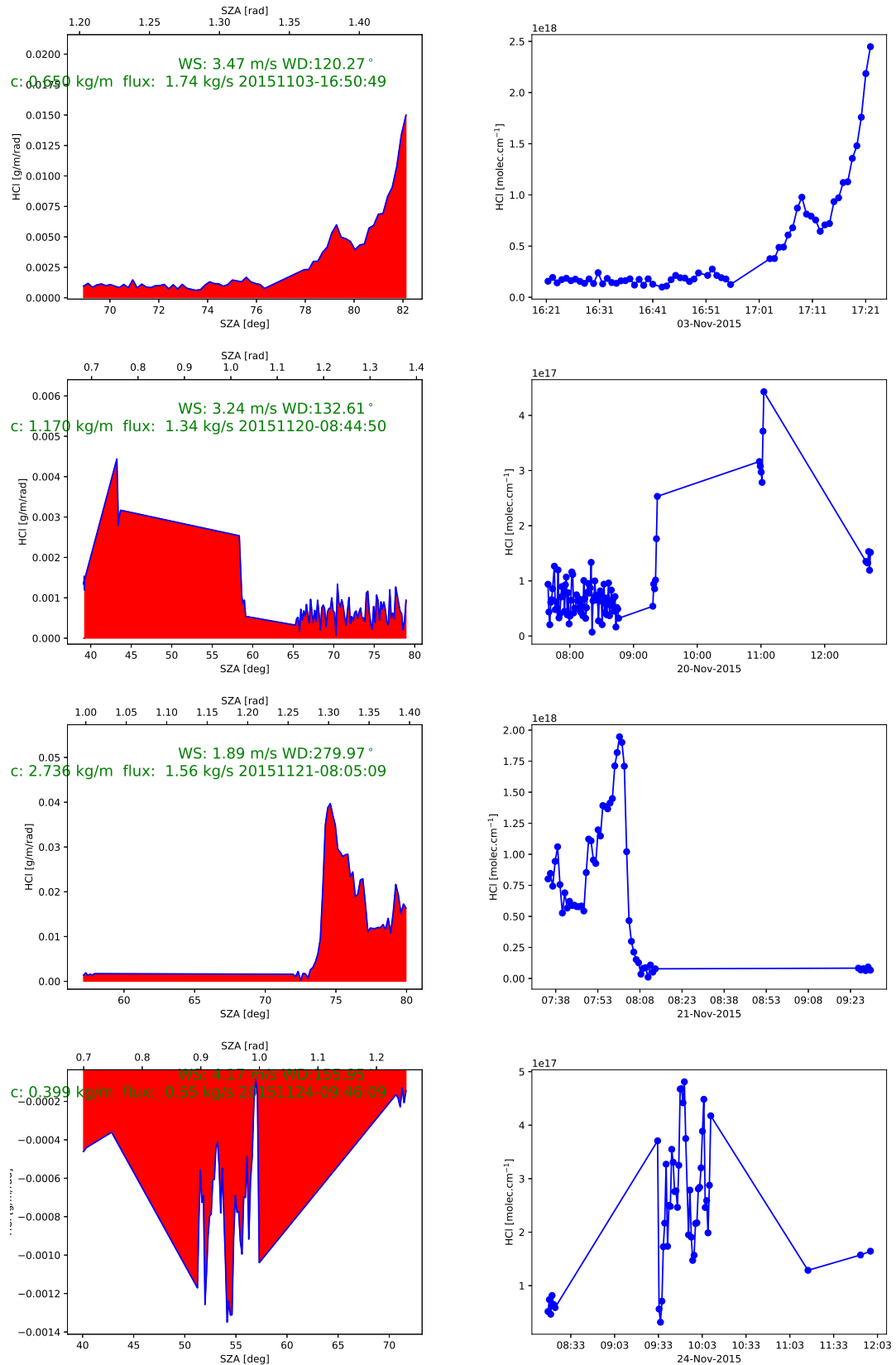












## REFERENCES

- Baylon, J. L., Stremme, W., Grutter, M., Hase, F., and Blumenstock, T. (2017). Background co<sub>2</sub> levels and error analysis from ground-based solar absorption ir measurements in central mexico. *Atmospheric Measurement Techniques Discussions* 2017, 1–18. doi:10.5194/amt-2016-418
- Butz, A., Dinger, A. S., Bobrowski, N., Kostinek, J., Fieber, L., Fischerkeller, C., et al. (2017). Remote sensing of volcanic co<sub>2</sub>, hf, hcl, so<sub>2</sub>, and bro in the downwind plume of mt. etna. *Atmospheric Measurement Techniques* 10, 1–14
- Keppel-Aleks, G., Toon, G. C., Wennberg, P. O., and Deutscher, N. M. (2007). Reducing the impact of source brightness fluctuations on spectra obtained by fourier-transform spectrometry. *Appl. Opt.* 46, 4774–4779. doi:10.1364/AO.46.004774
- Kiel, M., Wunch, D., Wennberg, P. O., Toon, G. C., Hase, F., and Blumenstock, T. (2016). Improved retrieval of gas abundances from near-infrared solar ftir spectra measured at the karlsruhe tccn station. *Atmospheric Measurement Techniques* 9, 669–682. doi:10.5194/amt-9-669-2016
- Taquet, N., Stremme, W., Baylon, J., Bezanilla, A., Schiavo, B., Rivera, C., et al. (2019). Variability in the gas composition of the popocatepetl volcanic plume. *Frontiers in Earth Science* 7, 114
- Wunch, D., Toon, G. C., Blavier, J.-F. L., Washenfelder, R. A., Notholt, J., Connor, B. J., et al. (2011). The total carbon column observing network. *Philosophical Transactions of the Royal Society of London A: Mathematical, Physical and Engineering Sciences* 369, 2087–2112

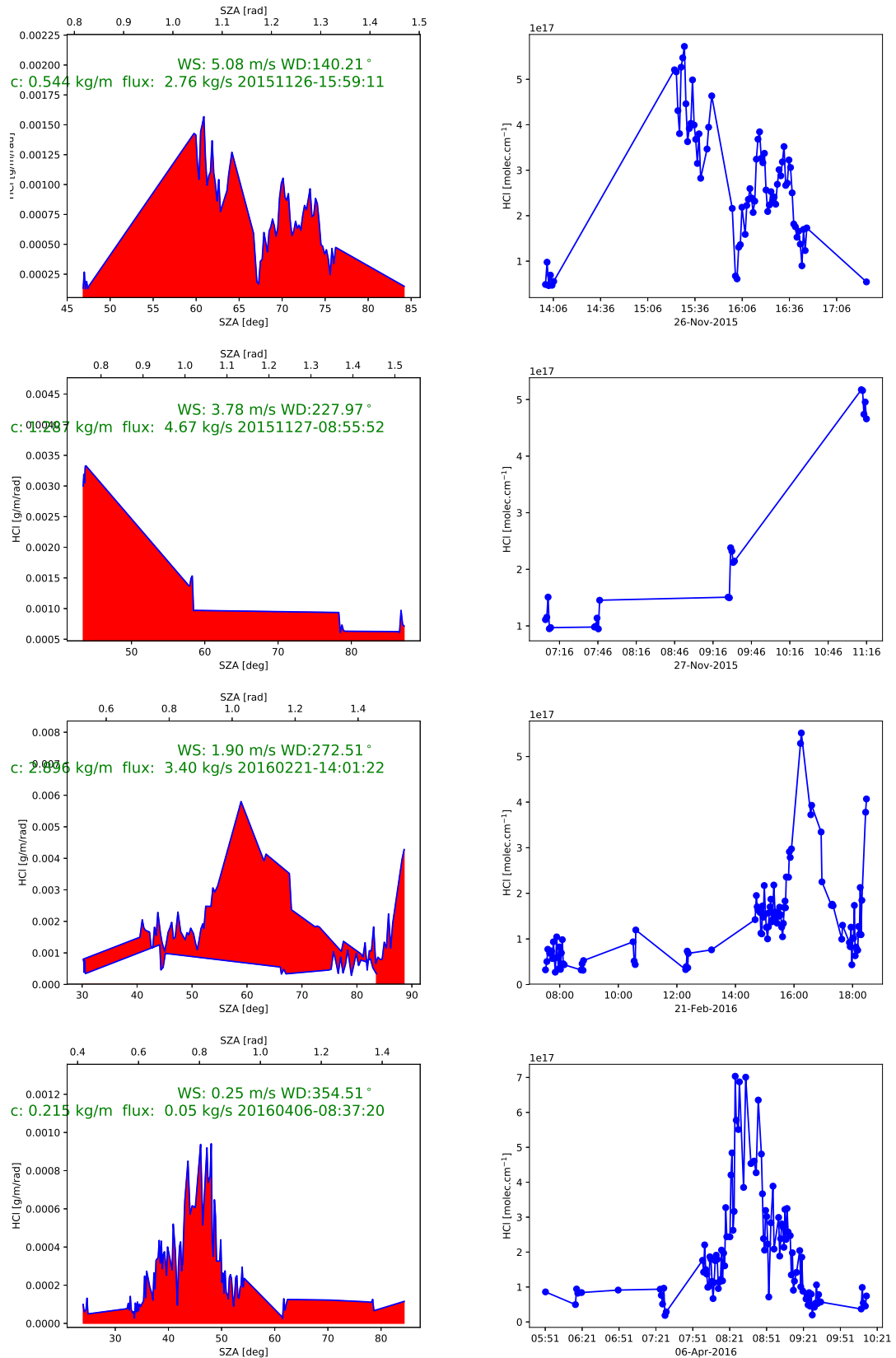


**Figure S27.** HCl plume cross section and time series: The geometrical reconstruction uses the wind direction and speed from reanalysis data with 3 hour time spacing. When the model is off or there are significant change in the wind direction, the estimated flux and cross section might result in unrealistic values, as a negative distance and cross section or similar indicators. These events are marked red in the table Tab.S2 and not used to calculate the mean flux.